Stem Cell Reports
Article

ISSCR

OPEN ACCESS

Dysregulation of the SIRT1/OCT6 Axis Contributes to Environmental Stress-Induced Neural Induction Defects

Guoping Li,[1] Zeyidan Jiapaer,[1] Rong Weng,[1] Yi Hui,[2] Wenwen Jia,[1] Jiajie Xi,[1] Guiying Wang,[1] Songcheng Zhu,[1] Xin Zhang,[2] Dandan Feng,[3,4] Ling Liu,[3,4] Xiaoqing Zhang,[3,4,5,*] and Jiuhong Kang[1,5,*]

[1]Clinical and Translational Research Center of Shanghai First Maternity and Infant Health Hospital, Shanghai Key Laboratory of Signaling and Disease Research, School of Life Science and Technology, Tongji University, 1239 Siping Road, Shanghai 200092, China
[2]Department of Anatomy and Neurobiology, The Jiangsu Key Laboratory of Neuroregeneration, Nantong University, Jiangsu 226001, China
[3]Institute of Translational Research, Tongji Hospital, Tongji University School of Medicine, Shanghai 200065, China
[4]Tongji University Advanced Institute of Translational Medicine
[5]The Collaborative Innovation Center for Brain Science, Tongji University
Shanghai 200092, China
*Correspondence: xqzhang@tongji.edu.cn (X.Z.), jhkang@tongji.edu.cn (J.K.)
http://dx.doi.org/10.1016/j.stemcr.2017.03.017

SUMMARY

Environmental stresses are increasingly acknowledged as core causes of abnormal neural induction leading to neural tube defects (NTDs). However, the mechanism responsible for environmental stress-triggered neural induction defects remains unknown. Here, we report that a spectrum of environmental stresses, including oxidative stress, starvation, and DNA damage, profoundly activate SIRT1, an NAD^+-dependent lysine deacetylase. Both mouse embryos and in vitro differentiated embryonic stem cells (ESCs) demonstrated a negative correlation between the expression of SIRT1 and that of OCT6, a key neural fate inducer. Activated SIRT1 radically deacetylates OCT6, triggers an OCT6 ubiquitination/degradation cascade, and consequently increases the incidence of NTD-like phenotypes in mice or hinders neural induction in both human and mouse ESCs. Together, our results suggest that early exposure to environmental stresses results in the dysregulation of the SIRT1/OCT6 axis and increases the risk of NTDs.

INTRODUCTION

Vertebrate embryonic development involves stepwise cell-fate conversion events. Neural induction is one of the most critical developmental events occurring during gastrulation, whereby a subset of epiblast cells acquires a neuroectodermal fate (Tam and Zhou, 1996). Neuroectodermal cells develop into all of the regional neural progenitors and ultimately the brain and spinal cord; thus, a failure of neural induction results in severe neural tube defects (NTDs) (Copp et al., 2003). Ninety percent of affected pregnancies will be terminated (Herrera-Araujo, 2016), with the survivors facing a risk of prenatal to postnatal lethality or lifelong disability, including neurological and cognitive complications. However, knowledge pertaining to abnormal neural induction in NTDs remains limited.

Previous studies have revealed that the suppression of bone morphogenetic protein (BMP) pathways and coordinated regulation of the fibroblast growth factor (FGF), transforming growth factor β, and calcineurin signaling pathways are central to the extrinsic control of neural induction (Cho et al., 2014; Liu et al., 2016a; Stavridis et al., 2007). These extracellular signals subsequently converge on specific lineage-determining transcription factors to regulate neural induction. For example, BMP/SMAD signaling suppresses commitment to the neural lineage via the induction of ID proteins (Ying et al., 2003a). The FGF-ERK1/2-PARP1 cascade directly activates *Pax6* expression to advance human neuroectodermal specification (Yoo et al., 2011; Zhang et al., 2010). Various transcription factors have also been found to lead undifferentiated cells to adopt a neural fate intrinsically. The zinc-finger nuclear protein *Zfp521* is required and sufficient to drive the intrinsic transition of embryonic stem cell (ESC) differentiation into neuroectodermal cells (Kamiya et al., 2011). The POU domain transcription factor *Oct6* initiates internal neural induction programs by directly activating neural-lineage genes, such as *Zfp521* and *Pax6* (Zhu et al., 2014), when expressed in the epiblast and the early neuroectoderm during development (Zwart et al., 1996). Disruption of the hierarchies of these signaling or gene-regulatory networks during early embryonic development may underlie abnormal neural induction in NTDs. Although NTDs have long been proposed to be primarily triggered by external environmental stresses, the specific environmental sensors that function to translate these environmental stresses into intracellular gene-regulatory network activity during the neural induction stage remain largely unexplored.

Sirt1, a conserved NAD^+-dependent lysine deacetylase, has been reported to be an environmental sensor that mediates intracellular responses to environmental states, such as redox state, nutrient availability, and DNA damage, in various organisms. In response to DNA damage or oxidative stress, *Sirt1* is activated to repress *p53*-dependent apoptosis in mammalian cells (Luo et al., 2001), nuclear

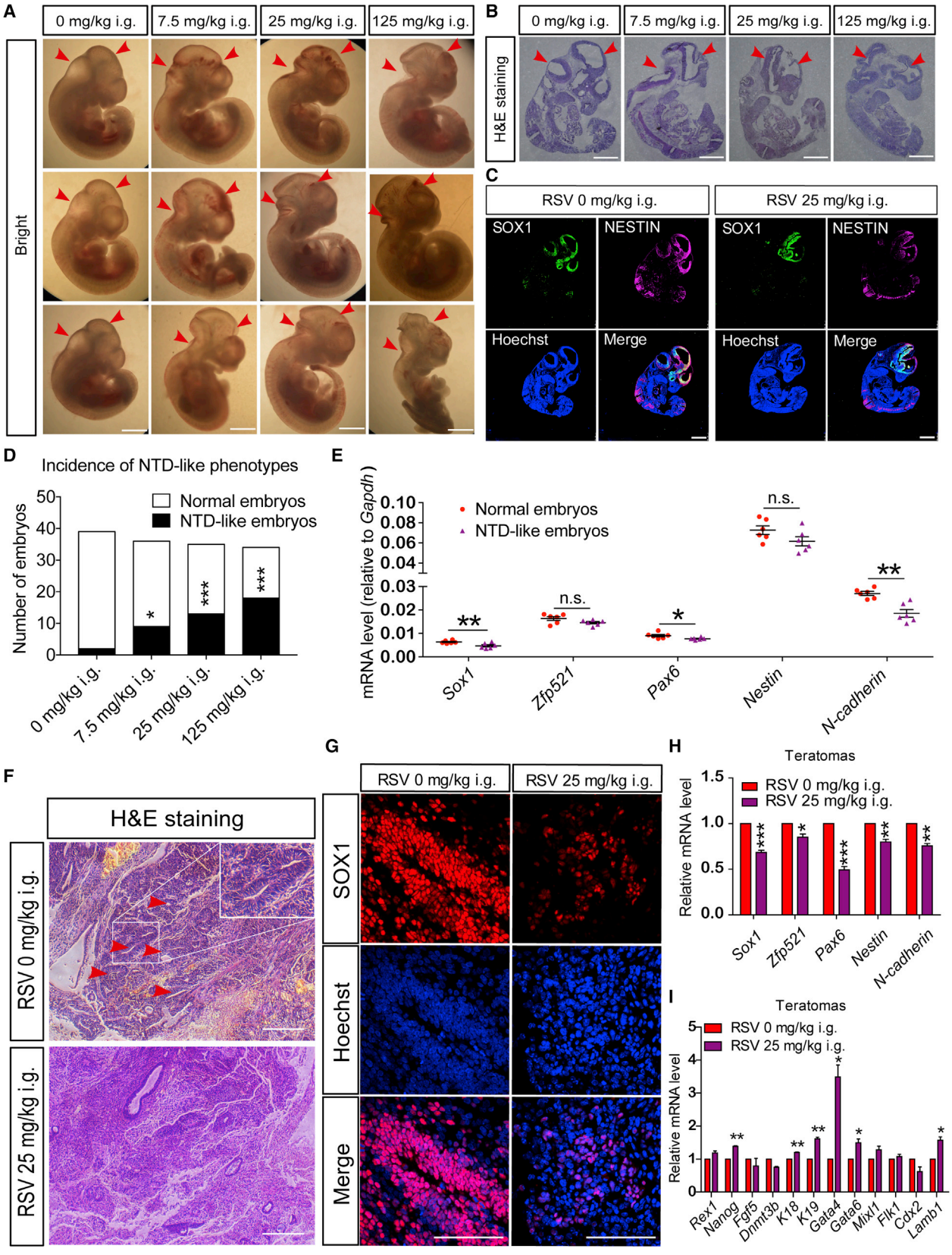

(legend on next page)

p53-mediated transactivation of proapoptotic genes in mouse cells (Han et al., 2008), and FOXO3-induced cell death in human cells (Brunet et al., 2004). Starvation-induced SIRT1 activation is required for the initiation of autophagy to cope with the lack of external nutrients in eukaryotes (Chang et al., 2015; Lee et al., 2008). Recently, *Sirt1* was also found to be required to suppress neurogenesis or to induce oligodendrogenesis in neural stem/progenitor cells (Prozorovski et al., 2008; Stein and Imai, 2014), suggesting a profound role for *Sirt1* during neural development.

Here, we report that environmental stresses activate SIRT1, which further deacetylates OCT6 and triggers an OCT6 ubiquitination/degradation cascade. Given that Oct6 is a crucial neural fate inducer during neural induction, environmental stress-triggered dysregulation of the SIRT1/OCT6 axis will therefore lead to neural induction defects and NTD-like phenotypes.

RESULTS

Early Maternal Exposure to Resveratrol Induces NTD-like Phenotypes in Mouse Embryos

SIRT1 has long been thought to be activated by environmental stresses to promote the survival of adult cells (Chang et al., 2015; Kang et al., 2009). As a potent SIRT1 activator, resveratrol (RSV) has been used to reveal various noteworthy features of SIRT1 deacetylase activity during numerous biological processes, including neurodegeneration and senescence (Pallas et al., 2009; Wood et al., 2004). To mimic environmental stress-induced SIRT1 activation during early neural development, we subjected pregnant mice to daily intragastric administration of RSV (25 mg/kg/day) between gestational day 3.5 (GD3.5) and GD10.5. When euthanized at GD10.5, 37.1% of the embryos that were exposed to RSV treatment displayed clear neurological malformations, exhibiting either a smaller brain size or increased indentations between the prosencephalon/metencephalon or metencephalon/spinal cord (Figures 1A, 1D, S1A, and S1B). No obvious morphological changes related to the heart primordium or the limb buds were found. Histological analysis and staining for SOX1 and NESTIN showed that the entire neural tube was severely misshapen and the neurocoele became smaller; these phenotypes resembled NTDs (Figures 1B and 1C). Consistent with the NTD phenotype, the expression of NTD-risk genes (*Gcn5*, *Folr1*, *Eya1*, *Six1*, *Alx1*, *Zic2*, *Acat2*, etc.) also showed obvious downregulation in the RSV-treated embryos (Figures S1C and S1D), which is consistent with their lower expression pattern or loss-of-function mutations in other NTD models or NTD patients (Fairbridge et al., 2010; Harris and Juriloff, 2010; Hsieh et al., 2013). Moreover, the expression of typical neural-lineage genes (*Sox1*, *Pax6*, and *N-cadherin*) was lower in RSV-treated embryos (Figure 1E). Even when the dosage of RSV was reduced to 7.5 mg/kg/day, 25% of the embryos still exhibited NTD-like phenotypes (Figures 1A, 1D, and S1A). Increasing the dosage to 125 mg/kg/day increased the incidence of NTD-like phenotypes to 52.9% (Figures 1A, 1D, and S1A). Similar results were obtained when RSV was intraperitoneally injected at GD3.5 until GD10.5 (Figures S1E and S1F). These data suggest that SIRT1 activation plays a detrimental role in early embryonic neural tube development.

RSV Causes NTD-like Phenotypes in Teratomas

The teratoma formation assay is another in vivo system that mimics early embryonic development. We subcutaneously injected mouse ESCs (mESCs) into NOD/SCID mice, followed by daily intragastric administration of RSV. Teratomas formed within 3–4 weeks and were then harvested for histological and mRNA analysis. Histological analysis and SOX1 immunostaining showed that teratomas from the RSV-treated group presented minimal neural tube-like structures (Figures 1F and 1G). mRNA analysis also revealed

Figure 1. RSV Induces NTD-like Phenotypes In Vivo

(A) Maternal intragastric (i.g.) RSV delivery from GD3.5 to GD9.5 induces dose-dependent NTD-like phenotypes in GD10.5 embryos. Red arrowheads indicate the prosencephalon/metencephalon and metencephalon/spinal cord junctions (also shown in B).

(B and C) Representative H&E staining (B) and SOX1 and NESTIN immunostaining (C) in frozen sections from the embryos in (A).

(D) Incidence of NTD-like phenotypes is positively correlated with RSV dosage.

(E) Neural-lineage gene expression between normal and RSV-induced NTD-like embryos.

(F) Teratomas obtained from mice after intragastric RSV administration show fewer neural tube-like structures. Red arrowheads indicate the neural tube-like structures.

(G) SOX1 staining of the teratomas in (F).

(H and I) Neural-lineage genes are expressed at lower levels in RSV-treated teratomas (H), but the expression of non-neural-lineage genes is upregulated (I).

Data are shown as means ± SEM of at least three independent experiments. The Chi-square test was used in (D), and unpaired two-tailed Student's t test was used in (H) and (I). n.s. (not significant), $p > 0.05$; *$p < 0.05$, **$p < 0.01$, ***$p < 0.001$ versus the control. Scale bars, 100 μm.

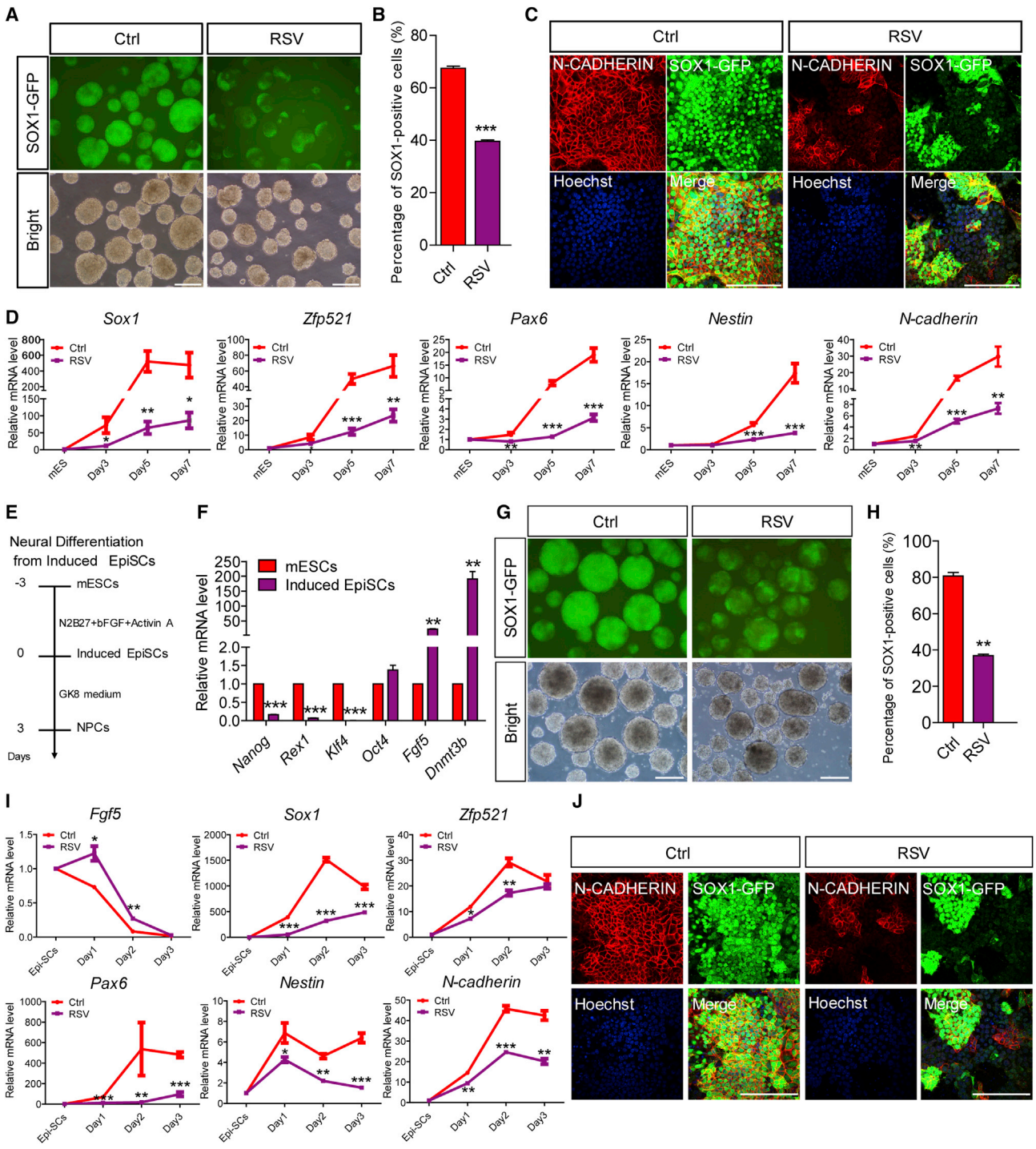

Figure 2. RSV Hinders the Neural Differentiation of mESCs and Induced EpiSCs In Vitro

(A and B) RSV (15 μM) treatment severely compromises the production of GFP$^+$ neural-lineage cells from mESCs, as shown by microscopy (A) and FACS (B) analysis in day-5 SFEBs.

(C) N-CADHERIN and GFP immunostaining of the cells in (A).

(D) RSV inhibits the expression of neural-lineage genes during the neural differentiation of mESCs.

(E) Schematic representation of the generation of induced EpiSCs and targeted neural differentiation in vitro.

(F) qPCR analysis of inner-cell-mass and epiblast markers between mESCs and induced EpiSCs.

(legend continued on next page)

that neural-lineage genes were expressed at lower levels (Figure 1H). In contrast, hallmark genes for pluripotency, endoderm, epidermis, and trophectoderm (*Nanog*, *Gata4*, *Gata6*, *K18*, *K19*, and *Lamb1*) were all upregulated (Figures 1I, S1G, and S1H). These results support a reduction of neural-lineage generation and a similar NTD-like phenotype in these RSV-treated teratomas.

RSV Hinders the Neural Induction of mESCs and Induced Epiblast Stem Cells In Vitro

To confirm the influence of SIRT1 activation on neural development, we selected a well-accepted system for the neural differentiation of mESCs in vitro involving serum-free cultured embryoid-body aggregates (SFEBs) (Watanabe et al., 2005). Using this system, mESCs were efficiently converted to a neural fate. This result was demonstrated by the sequential downregulation and activation of pluripotent genes, epiblast genes, neural-lineage genes, and neuronal genes during neural differentiation (Figure S2A). In addition, as 46C is a *Sox1-GFP* reporter line (Ying et al., 2003b), GFP expression faithfully recapitulated endogenous *Sox1* expression and indicated a committed neural fate (Figures S2A–S2C). All of these observations suggest the usefulness of this in vitro differentiation system for mimicking dynamic neural developmental events.

When RSV was applied to neural differentiation medium, the generation of GFP^+ neural-lineage cells was severely compromised in a dose-dependent manner (Figures 2A, 2B, and S2D). Immunostaining assays confirmed the reduced percentage of SOX1-GFP^+/N-$CADHERIN^+$ or $SOX1^+$/$NESTIN^+$ neural stem/progenitor cells generated in the RSV-treated group (Figures 2C, S2E, and S2F). qPCR analysis revealed that *Sox1*, *Zfp521*, *Pax6*, *Nestin*, and *N-cadherin* mRNA levels were all significantly reduced after RSV treatment (Figure 2D). We also confirmed that RSV treatment slightly affected the apoptosis or cell cycle of differentiated mESCs (Figures S2G and S2H). Additionally the mRNA levels of pluripotent genes (*Nanog* and *Rex1*), epiblast genes (*Fgf5* and *Dnmt3b*), mesodermal genes (*Mixl1* and *Flk1*), endodermal genes (*Gata4* and *Gata6*), trophectodermal genes (*Cdx2* and *Lamb1*), and epidermal genes (*K18* and *K19*) were all increased after RSV treatment (Figure S2I). Similar results were obtained in another mESC line, R1 (Figures S2J and S2K). These data suggest that early exposure to SIRT1 activation preferentially hinders the neural-lineage specification of mESCs by maintaining mESCs in a pluripotent state or forcing the cells to adopt a non-neural fate in vitro.

To identify the SIRT1 activation-sensitive stage during neural differentiation, we applied RSV to differentiated mESCs at different time points until day 5, when the mESCs were mostly committed to neural progenitors under normal differentiation conditions. The most significant suppression of neural differentiation was achieved when RSV was added from day 0, 1 or 2, but not afterward (Figures S3A–S3C). Short-term RSV treatment from days 0–3 or days 2–3 also significantly inhibited neural differentiation (Figures S3D–S3F). These data suggest that differentiated mESCs are most sensitive to SIRT1 activation on days 2–3, defined as the neural induction period. Furthermore, similar neural induction defects were observed when RSV was applied to induced epiblast stem cells (EpiSCs) (Figures 2E–2J). These results demonstrate that SIRT1 activation specifically hinders the neural induction process.

RSV Inhibits the Neural Induction of mESCs in a SIRT1 Deacetylase Activity-Dependent Manner

To confirm the role of SIRT1 deacetylase activity in RSV treatment-induced neural induction defects, we first treated mESCs with RSV for 1.5 or 2.5 days under differentiation conditions and then collected the cells for western blotting. A remarkable decrease in the levels of acetylated H4K16 and H3K9, the two best-known SIRT1 histone targets, was observed after RSV treatment, whereas no obvious influences on other potential targets of RSV (e.g., GSK3β or ERK1/2 signaling) were detected (Figure 3A). We also immunoprecipitated SIRT1 from day-2.5 SFEBs in the absence or presence of RSV treatment, and examined SIRT1 deacetylase activity. The results showed that SIRT1 deacetylase activity was upregulated by more than 7-fold after RSV exposure, without obvious changes in SIRT1 protein levels (Figures 3B and S4A). Furthermore, as we expected, activating SIRT1 deacetylase using another potent activator, SRT1720, similarly inhibited the neural differentiation of 46C mESCs (Figures 3C, 3D, and S4B). These observations prove that SIRT1 deacetylase activation is sufficient to trigger neural induction defects.

Next, we used two efficient short hairpin RNAs (shRNAs) against the coding region of *Sirt1* to knock down *Sirt1*, along with a control shRNA against *Luciferase* (sh*Luc*) (Figures S4C and S4D). sh*Luc* and sh*Sirt1* mESCs were then subjected to neural differentiation for 5 days in the absence or

(G and H) RSV treatment (15 μM) severely compromises the production of neural-lineage cells from induced EpiSCs, as shown by microscopy (G) and FACS (H) analysis in day-3 SFEBs from induced EpiSCs.

(I) RSV inhibits the expression of neural-lineage genes during the neural differentiation of induced EpiSCs.

(J) N-CADHERIN and GFP immunostaining of the cells in (G).

Ctrl, control (and similarly hereafter). Data are shown as means ± SEM of three independent experiments. Unpaired two-tailed Student's t test. *p < 0.05, **p < 0.01, ***p < 0.001 versus the control. Scale bars, 100 μm.

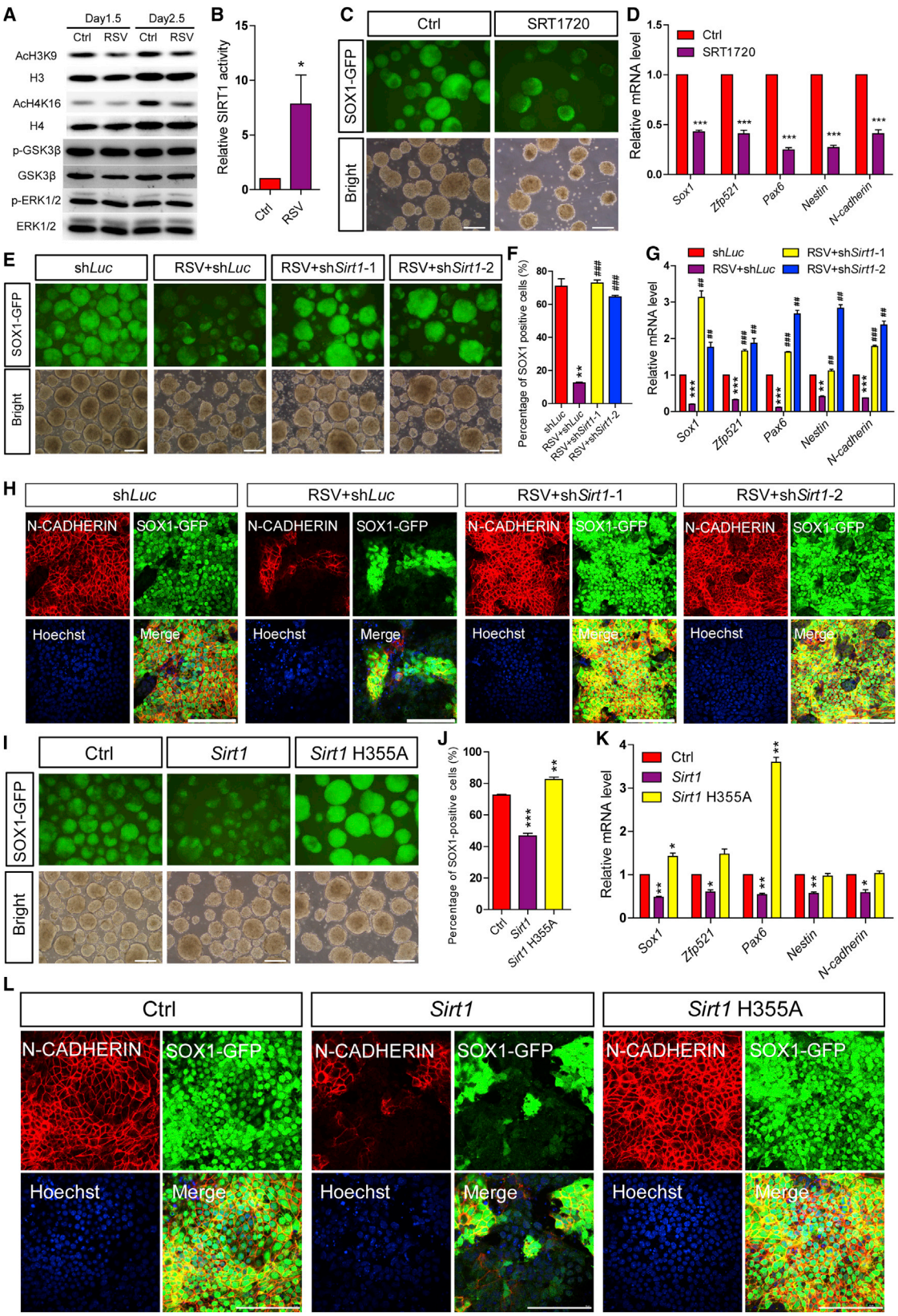

(legend on next page)

presence of RSV treatment. Similar to wild-type mESCs, RSV-treated sh*Luc* mESCs showed a lower efficiency of neural induction (Figures 3E–3H), whereas *Sirt1* knockdown clearly potentiated the efficiency of neural induction in both the absence and presence of RSV treatment (Figures 3E–3H and S4E–S4G). Considering the pattern of decreased *Sirt1* expression during normal neural differentiation (Figures S4H and S4I), we revealed that the downregulation of SIRT1 deacetylase activity is a prerequisite for the efficient conversion of pluripotent stem cells to a neural fate during gastrulation. Through CRISPR/Cas9-mediated homologous recombination, we further integrated CAG promoter-driven wild-type *Sirt1* or a deacetylase-inactive *Sirt1* mutant (*Sirt1* H355A) into the *Hprt* locus for constitutive overexpression in mESCs (Cong et al., 2013; Koyama et al., 2006; Liu et al., 2016a). The overexpression efficiency was examined by qPCR and western blotting (Figures S4J and S4K). Overexpressing wild-type *Sirt1* significantly retarded neural induction, whereas overexpressing the *Sirt1* H355A mutant slightly potentiated rather than suppressed the efficiency of neural induction (Figures 3I–3L). Collectively our results indicate that RSV hinders the neural induction of mESCs in a SIRT1 deacetylase activity-dependent manner.

SIRT1 Directly Targets OCT6 and Then Activates Its Deacetylation/Ubiquitination/Degradation Cascade

Neural induction is tightly controlled by key neuroectodermal transcription factors, including *Sox2*, *Otx2*, *Zic2*, *Pax6*, and *Oct6* (Acampora et al., 2013; Nagai et al., 2000; Zhang et al., 2010; Zhou et al., 2016; Zhu et al., 2014). To determine which transcription factors were responsible for the SIRT1 activation-induced neural induction defects, we overexpressed these transcription factors in RSV-treated mESCs, whereby only *Oct6* overexpression improved the neural induction efficiency (Figures 4A–4C and S5A). Given that *Oct6* initiates the neural induction program via direct activation of *Zfp521*, we found that overexpression of *Zfp521* completely rescued the neural induction defects triggered by RSV treatment (Figures S5B–S5D), indicating that the *Oct6*/*Zfp521* axis may be responsible for the SIRT1 activation-triggered neural induction defects. Interestingly, examining the mRNA and protein levels of *Oct6* revealed that RSV markedly downregulated OCT6 protein expression, while the mRNA level remained unchanged (Figures 4D and 4E). Moreover, OCT6 enrichment in the enhancer regions of hallmark neural-lineage genes such as *Zfp521* and *Pax6* was also significantly decreased after RSV treatment (Figure 4F). These data suggested that SIRT1 activation might decrease OCT6 protein stability at the post-translational level, which thereby leads to the neural induction defects. To this end, we examined OCT6 expression levels in sh*Sirt1* mESCs and found that *Sirt1* knockdown upregulated OCT6 protein levels, but not *Oct6* mRNA levels, in mESCs (Figures 4G and S5E) and rescued RSV-triggered OCT6 downregulation (Figures 4H and S5F). Furthermore, overexpression of wild-type *Sirt1* but not the deacetylase-inactive mutant (*Sirt1* H355A) decreased OCT6 protein expression (Figures 4I and S5G). All of these data suggest that the deacetylase activity of SIRT1 is negatively correlated with OCT6 protein stability.

Pretreatment with a potent proteasome inhibitor, MG132, stabilized OCT6 protein expression in the presence of RSV treatment (Figure 4J), indicating that the ubiquitin-proteasome pathway is involved in RSV-triggered OCT6 degradation. Immunoprecipitation using an acetylated lysine (Ac-Lys) antibody was then performed in day-2.5 SFEBs after pretreatment with MG132, for which the results showed that the acetylation of OCT6 was eliminated by RSV treatment (Figure 4K). In addition, RSV treatment induced robust ubiquitination of OCT6 (Figure 4L), consistent with the hypothesis that SIRT1 activation triggers the deacetylation/ubiquitination/degradation cascade of OCT6.

To verify the physical interaction between SIRT1 and OCT6, we pulled down endogenous SIRT1 in day-2.5 SFEBs and performed western blotting, which showed substantial amounts of OCT6 in the immunocomplexes (Figure 4M). Overexpression of *Flag*-tagged *Sirt1* and *hemagglutinin* (*HA*)-tagged *Oct6* in HEK 293FT cells also revealed strong

Figure 3. RSV Inhibits the Neural Differentiation of mESCs in a SIRT1 Deacetylase Activity-Dependent Manner

(A) RSV treatment causes an obvious decrease in acetylated H4K16 and H3K9 but does not alter phosphorylated GSK3β and ERK1/2, as shown by western blotting of day-1.5 and day-2.5 SFEBs.

(B) SIRT1 deacetylase activity shows a dramatic increase upon RSV treatment in day-2.5 SFEBs.

(C and D) SRT1720 treatment (1.5 μM) inhibits the neural differentiation of mESCs, as shown by microscopy (C) and qPCR (D) analysis in day-5 SFEBs.

(E–H) *Sirt1* knockdown potentiates the RSV-suppressed neural induction efficiency, as shown by microscopy (E), FACS (F), qPCR (G), and immunostaining (H) analysis in day-5 SFEBs.

(I–L) Ectopic expression of *Sirt1*, but not *Sirt1* H355A mutant, inhibits the neural differentiation of mESCs, as shown by microscopy (I), FACS (J), qPCR (K), and immunostaining (L) analysis in day-5 SFEBs.

Data are shown as means ± SEM of three independent experiments. Unpaired two-tailed Student's t test. *p < 0.05, **p < 0.01, ***p < 0.001 versus the control; $^{\#\#}$p < 0.01, $^{\#\#\#}$p < 0.001 versus the RSV-treated sh*Luc* group. Scale bars, 100 μm.

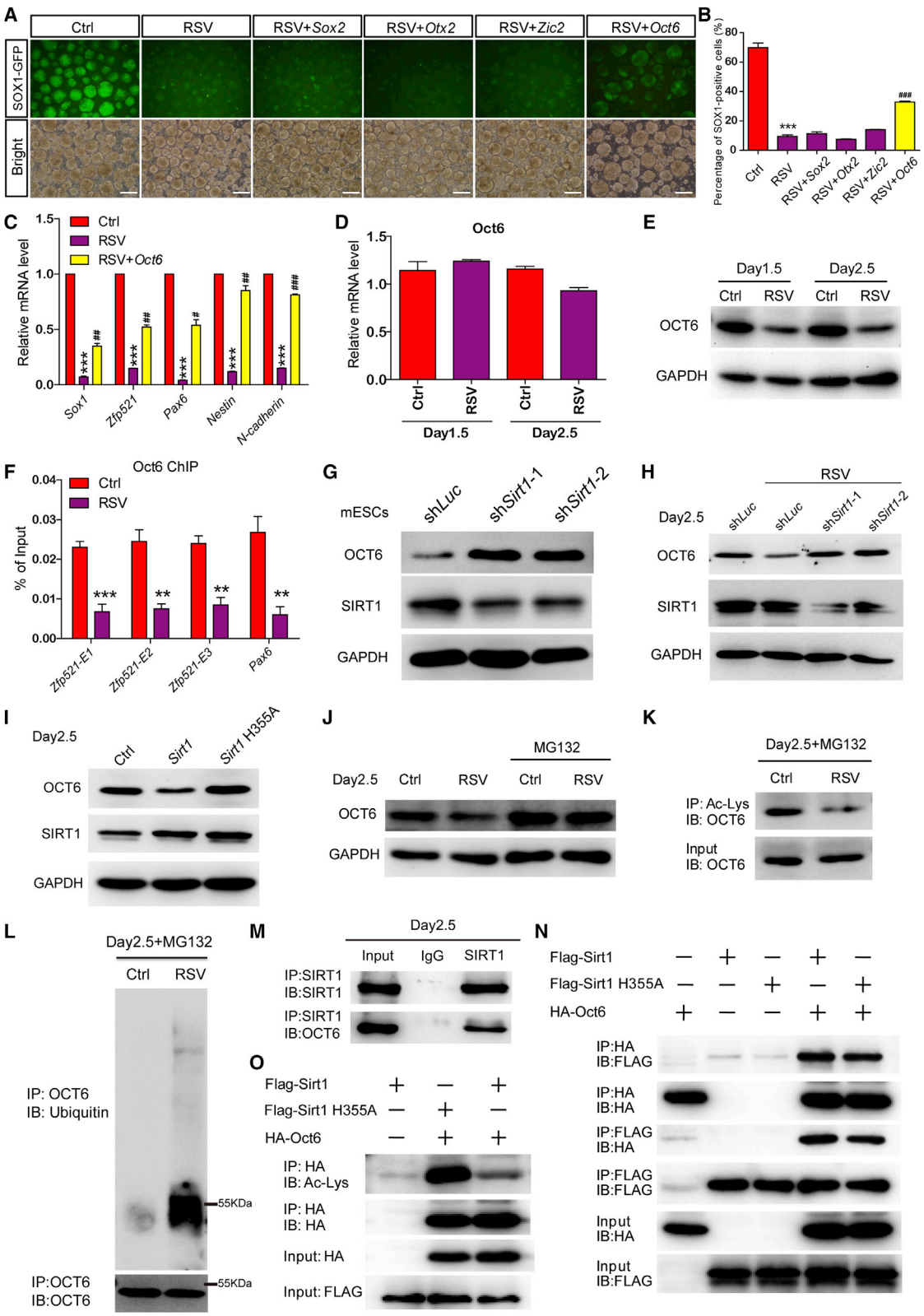

(legend on next page)

binding of exogenous SIRT1 and OCT6 (Figure 4N). Moreover, SIRT1 H355A mutant showed an efficient interaction with OCT6 (Figure 4N), indicating that the deacetylase activity of SIRT1 is not required for the physical interaction between SIRT1 and OCT6, whereas the overexpression of wild-type SIRT1 resulted in significant deacetylation of OCT6 compared with the overexpression of the SIRT1 H355A mutant in HEK 293FT cells (Figure 4O). Furthermore, when the OCT6 K263&268Q mutant, which mimics constitutively acetylated OCT6 by mutating the two putative SIRT1-deacetylated lysine residues to glutamine, was overexpressed along with differentiation, RSV treatment failed to interfere with the neural induction of mESCs (Figures S5H–S5J). These data confirm that SIRT1 directly targets and deacetylates OCT6 to activate its ubiquitination/degradation cascade.

Oct6 Is Required for Neural Induction

A previous study established that mESCs in which *Oct6* is knocked down tend to show decreased neural fate commitment (Zhu et al., 2014). To confirm that *Oct6* indeed plays an essential role in neural induction, we generated *Oct6*$^{-/-}$ mESCs via CRISPR/Cas9-mediated open reading frame deletion (Liu et al., 2016b) (Figure S5K). Knockout efficiency was confirmed via genomic DNA PCR, western blotting, and qPCR (Figures S5K–S5N). After being subjected to neural differentiation, the *Oct6*$^{-/-}$ mESCs failed to efficiently convert to neuroectodermal cells, as demonstrated by much lower GFP induction and the reduced expression of neural-lineage-specific genes (Figures S5O–S5Q). In addition, reintroducing *Oct6* into the *Oct6*$^{-/-}$ mESCs rescued the neural induction efficiency (Figures S5O–S5Q), confirming that the neural induction defects are correlated with a lack of OCT6 expression. As described above, *Sirt1* knockdown in 46C mESCs potentiated neural induction. We next knocked down *Sirt1* in *Oct6*$^{-/-}$ mESCs and found that *Sirt1* knockdown failed to ameliorate the neural induction defects (Figure S5R). These results provide further evidence that OCT6 acts as a downstream target of SIRT1 and that the SIRT1/OCT6 axis determines neural induction from pluripotent stem cells.

The SIRT1/OCT6 Axis Is Responsible for Environmental Stress-Induced Neural Induction Defects

Epidemiological studies have implied that environmental stresses might serve as risk factors for NTDs (Salih et al., 2014). To examine whether environmental stresses indeed affect neural development, we treated mESCs with the reactive oxygen species inducer H_2O_2 or the DNA damage inducer hydroxyurea (HU), or starved cells via glucose withdrawal for 24 hr during the neural induction stage (approximate neural differentiation days 1.5–2.5). Remarkably, all of these environmental stresses significantly hindered neural induction and instead forced mESCs to adopt a non-neural fate or maintained the cells in a pluripotent stage under differentiation conditions (Figures 5A–5C and S6A). Considering that SIRT1 is usually activated by environmental stresses, we first analyzed SIRT1 deacetylase activity after stimulation to determine whether these environmental stresses interfered with neural induction by targeting the SIRT1/OCT6 axis. As with RSV treatment, SIRT1 deacetylase activity was significantly elevated under all the examined environmental stress conditions (Figures 5D and S6B). Western blotting showed that H_2O_2, HU, and glucose starvation also greatly downregulated OCT6 protein levels, but not its transcript (Figures 5E and S6C). Next, we studied the effects of H_2O_2 and HU exposure, as well as glucose starvation, in sh*Sirt1* mESCs. In contrast to the sh*Luc* mESCs, sh*Sirt1* mESCs normally differentiated

Figure 4. SIRT1 Directly Targets OCT6 and Then Activates Its Deacetylation/Ubiquitination/Degradation Cascade

(A and B) Overexpression of *Oct6*, but not *Sox2*, *Otx2*, or *Zic2*, ameliorates the RSV-induced neural induction defects, as shown by microscopy (A) and FACS (B) analysis.

(C) qPCR confirmed the amelioration of neural induction defects via Oct6 overexpression.

(D and E) OCT6 protein (E), rather than *Oct6* mRNA (D), is downregulated after RSV treatment during neural induction.

(F) OCT6 enrichment in the enhancer regions of *Zfp521* and *Pax6* is greatly compromised in RSV-treated day-2.5 SFEBs.

(G) *Sirt1* knockdown elevates OCT6 protein levels in mESCs.

(H) *Sirt1* knockdown rescues the downregulation of OCT6 protein expression in RSV-treated day-2.5 SFEBs.

(I) Overexpression of *Sirt1*, but not *Sirt1* H355A mutant, downregulates OCT6 protein levels in day-2.5 SFEBs.

(J) MG132 pretreatment stabilizes OCT6 protein in RSV-treated day-2.5 SFEBs.

(K and L) Immunoprecipitation of MG132-pretreated SFEBs with anti-Ac-Lys (K) or anti-OCT6 (L), followed by blotting with anti-OCT6 (K) and anti-ubiquitin (L).

(M) SIRT1 endogenously interacts with OCT6 in day-2.5 SFEBs.

(N) HA-tagged OCT6 directly interacts with FLAG-tagged SIRT1 or SIRT1 H355A when co-transfected into HEK 293FT cells.

(O) The acetylation of OCT6 is decreased when SIRT1 is co-transfected into HEK 293FT cells compared with the SIRT1 H355A mutant.

IP, immunoprecipitate; IB, immunoblot. Data are shown as means ± SEM of three independent experiments. Unpaired two-tailed Student's t test. $^{**}p < 0.01$, $^{***}p < 0.001$ versus the control; $^{\#}p < 0.05$, $^{\#\#}p < 0.01$, $^{\#\#\#}p < 0.001$ versus the RSV-treated blank vector group. Scale bars, 100 μm.

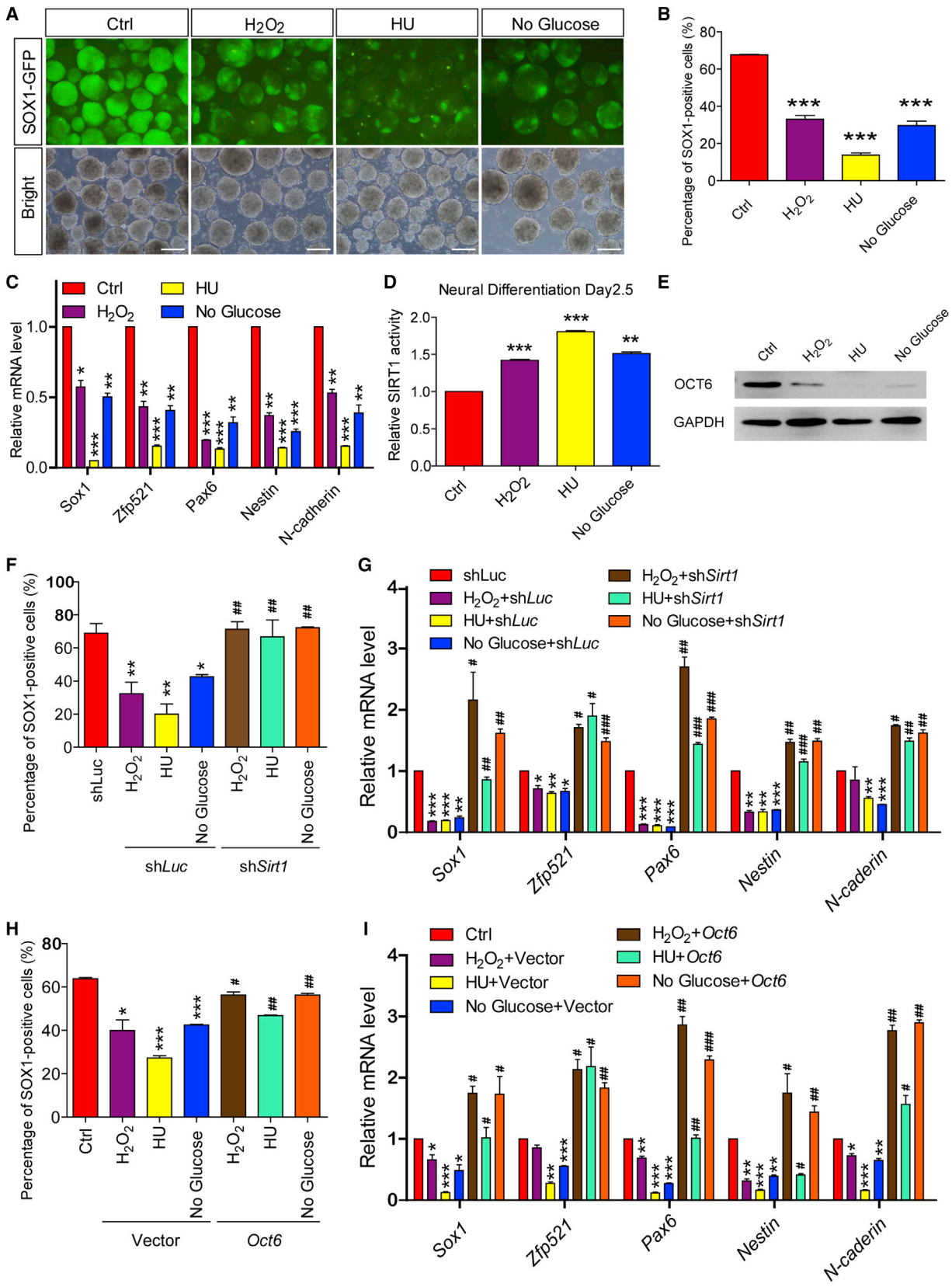

(legend on next page)

into neuroectodermal cells when challenged with these environmental stresses (Figures 5F, 5G, and S6D). Similarly, ectopic *Oct6* expression also ameliorated the neural induction defects induced by these environmental stresses (Figures 5H, 5I, and S6E). Taken together, these results confirm that the SIRT1/OCT6 axis is responsible for the neural induction defects triggered by these environmental stresses.

Environmental Stresses Equally Target the SIRT1/OCT6 Axis and Retard Neural Induction in Human Embryonic Stem Cells

To determine whether environmental stresses also target the SIRT1/OCT6 axis and thereby cause neural induction defects in humans, we performed teratoma formation assays by injecting human ESCs (hESCs) into the immunodeficient mice in the absence or presence of daily RSV administration (50 mg/kg/day intragastrically). After 2 months, teratomas were harvested for histological and mRNA analysis. Similar to the data obtained from mouse teratomas, we found that neural-lineage induction was significantly hindered and that the populations of other layers as well as pluripotent cells were elevated after RSV administration (Figures S7A–S7C).

Next, we employed our well-established neural differentiation paradigm (Chi et al., 2016; Zhang and Zhang, 2010), with which hESCs can be efficiently converted into neuroectodermal cells uniformly expressing *Sox1*, *Sox2*, *Nestin*, and *N-cadherin* (Figures 6A and 6B, left panel). Supplementing the differentiation medium with RSV severely retarded the expression of all of these neural-lineage genes at both the protein and mRNA levels, with elevated expression of other non-neural-lineage genes (Figures 6A–6C and S7D). Consistently, RSV treatment markedly elevated SIRT1 deacetylase activity (Figures 6D and S7E) and decreased *Oct6* expression at the protein level rather than the mRNA level (Figures 6E and S7F). All of these results suggest that the role of the SIRT1/OCT6 axis is potentially conserved between mice and humans. To this end, we knocked out *Sirt1* in hESCs via the CRISPR/Cas9 system (Liu et al., 2016b) (Figure S7G) and subjected the cells to neural differentiation. Accordingly, we observed dramatically elevated OCT6 protein levels in *Sirt1*$^{-/-}$ hESCs during the early neural differentiation stage, when no OCT6 protein was detected in wild-type hESCs (Figure 6F). As neural differentiation proceeded, improved neural induction efficiency was observed in *Sirt1*$^{-/-}$ hESCs (Figure 6G). We next induced the neural induction of *Sirt1*$^{-/-}$ hESCs in the presence of RSV treatment. Accordingly, *Sirt1*$^{-/-}$ hESCs were resistant to the RSV-induced degradation of OCT6 protein and underwent normal neural induction under RSV exposure (Figures 6H and 6I). In addition, *Sirt1* overexpression, H_2O_2 or HU treatment, and glucose starvation retarded the neural induction of hESCs in similar fashion (Figures 6J, 6K, S7H, and S7I). Collectively these observations suggest that the functional role of the SIRT1/OCT6 axis, which is responsible for environmental stress-triggered neural induction defects, is conserved between mice and humans.

The Functional Role of the SIRT1/OCT6 Axis in Environmental Stress-Induced NTDs during Early Embryogenesis

To confirm the physiological relevance of the SIRT1/OCT6 pathway in vivo, we first stained GD3.5 and GD6.5 embryos for SIRT1 and OCT6 and found that OCT6 protein levels were greatly upregulated at GD6.5 during normal gastrulation, which was accompanied by a significant decrease in SIRT1 expression (Figures 7A and 7B). In addition, *Sirt1*$^{+/-}$ embryos (*Sirt1*$^{fl/fl}$ mice crossed with *EIIa-Cre* mice) showed an obvious elevation in OCT6 protein levels (Figure 7C), indicating that SIRT1 negatively regulates OCT6 during normal embryonic development. To verify the role of SIRT1 in RSV-induced NTD-like phenotypes, we treated wild-type and *Sirt1*$^{+/-}$ embryos with RSV from GD3.5 to GD10.5. We found that 29.4% of wild-type embryos displayed NTD-like phenotypes, compared with only 5.8% of Sirt1$^{+/-}$ embryos (Figure 7D). Similarly, OCT6 protein levels were significantly decreased in wild-type embryos, whereas this decrease was obviously compromised in *Sirt1*$^{+/-}$ embryos at GD6.5 (Figure 7E).

Figure 5. The SIRT1/OCT6 Axis Is Responsible for Environmental Stress-Induced Neural Induction Defects

(A–C) H_2O_2 (0.4 mM), HU (0.4 μM), and glucose starvation hinder the neural induction of mESCs, as shown by microscopy (A), FACS (B), and qPCR (C) analysis of day-5 SFEBs.

(D) SIRT1 deacetylase activity is significantly propagated under H_2O_2, HU, and glucose starvation conditions.

(E) OCT6 protein is greatly downregulated under H_2O_2, HU, and glucose starvation conditions.

(F and G) *Sirt1* knockdown rescues the neural induction defects triggered by H_2O_2, HU, and glucose starvation, as shown by FACS (F) and qPCR (G) analysis of day-5 SFEBs.

(H and I) *Oct6* overexpression rescues the neural induction defects triggered by H_2O_2, HU, and glucose starvation, as shown by FACS (H) and qPCR (I) analysis of day-5 SFEBs.

Data are shown as means ± SEM of three independent experiments. Unpaired two-tailed Student's t test. *$p < 0.05$, **$p < 0.01$, ***$p < 0.001$ versus the untreated control; $^{\#}p < 0.05$, $^{\#\#}p < 0.01$, $^{\#\#\#}p < 0.001$ versus the sh*Luc* group (F and G) or the blank vector group (H and I) under the same challenge conditions. Scale bars, 100 μm.

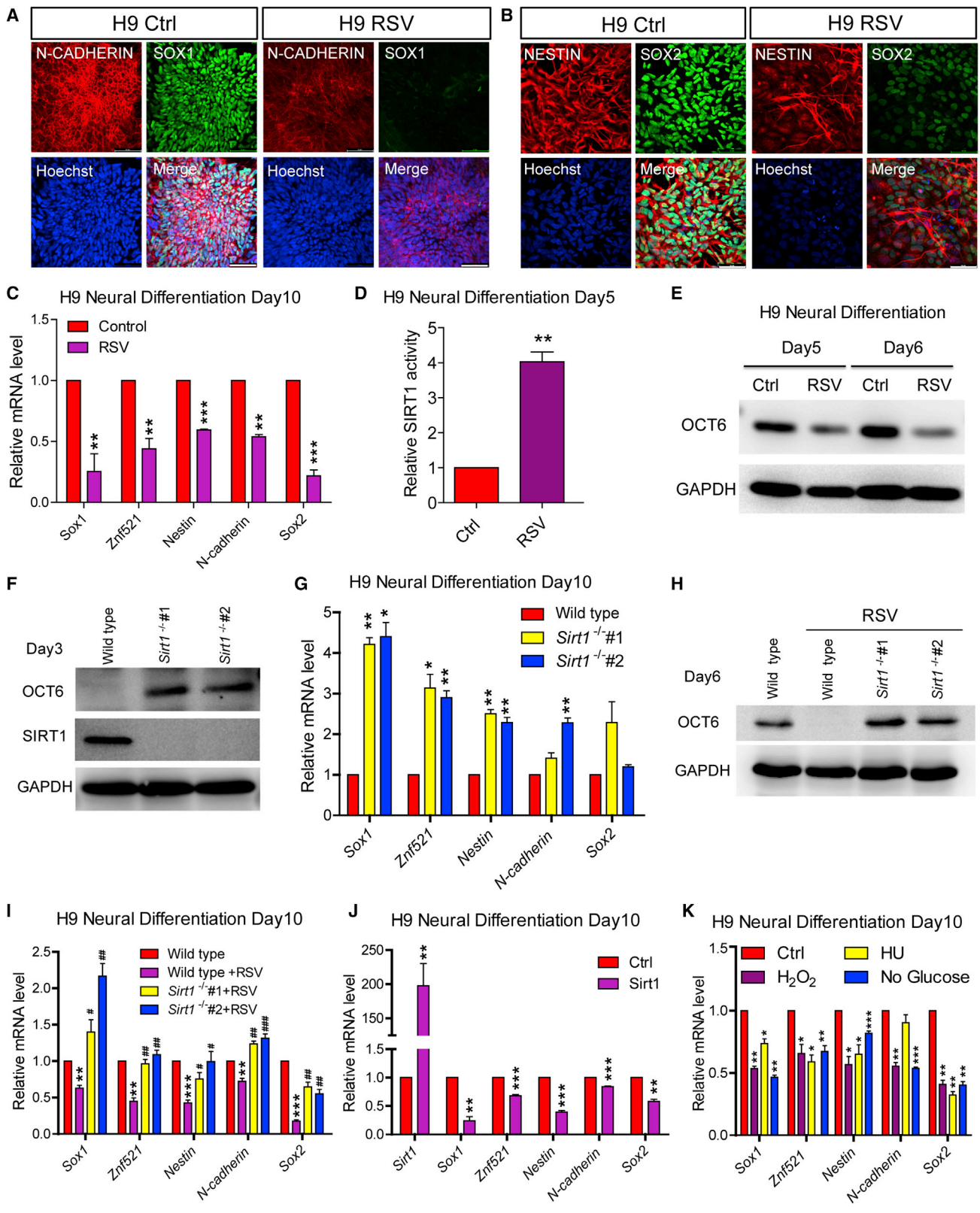

(legend on next page)

Interestingly, brain-specific heterozygous *Sirt1* knockout embryos (*Sirt1*$^{fl/fl}$ mice crossed with *Nestin-Cre* mice) showed a similar incidence of NTD-like phenotypes in wild-type embryos after maternal RSV administration (Figure 7D). *Nestin* is a neural-lineage-specific gene that is activated at approximately GD7.5. We then applied RSV starting at different gestational days until GD10.5. The results showed that RSV exposure from GD3.5, GD4.5, GD5.5, and GD6.5, but not afterward, efficiently induced NTD-like phenotypes; a single RSV administration at GD6.5 also induced NTD-like phenotypes (Figure 7F). Together, these results demonstrate that RSV/SIRT1/OCT6 pathway-triggered NTDs occur early on during neural induction, before the neural lineages have been specified. Indeed, we observed overlapping SIRT1 and OCT6 expression, the physical interaction between these two proteins, as well as the acetylation of OCT6 protein, at this developmental stage (Figures 7B, 7G, and S7J).

To recapitulate the functional role of the SIRT1/OCT6 pathway in environmental stress-induced NTDs, we employed radiation-induced NTDs as a pathophysiologically relevant in vivo model for NTDs. After 4 Gy radiation at GD5.5, 28.5% of wild-type embryos displayed NTD-like phenotypes, compared with only 6.8% of *Sirt1*$^{+/-}$ embryos (Figures 7H and S7K). Furthermore we found that after irradiation, OCT6 protein levels were significantly decreased in wild-type embryos, whereas this decrease was obviously compromised in *Sirt1*$^{+/-}$ embryos at GD6.5 (Figure 7I). Collectively, these data support the pathophysiological role of the SIRT1/OCT6 axis in environmental stress-induced NTDs (Figure 7J).

DISCUSSION

In this study, we report an evolutionarily conserved SIRT1/OCT6 axis that is involved in abnormal neural induction in NTDs. RSV, oxidative stresses, starvation, and DNA damage inducers all activate SIRT1 deacetylase activity, which radically deacetylates OCT6 and triggers its ubiquitination/degradation cascade. Importantly, the dysregulation of the SIRT1/OCT6 axis will thereby induce NTD-like phenotypes in mice or hinder the neural induction of both hESCs and mESCs. Collectively, our data shed light on a pathophysiologically relevant role of the SIRT1/OCT6 axis in environmental stress-induced NTDs.

Annually, more than 300,000 neonates are born with NTDs worldwide. The risk of NTDs has long been proposed to be increased by environmental stresses, including maternal starvation, fever, and exposure to radiation or other teratogens, while the potential messenger between environmental stresses and NTDs remains unknown. SIRT1 has been reported to regulate the fate decision of neural stem/progenitor cells in response to environmental stimuli (Stein and Imai, 2014). However, NTDs arise when the process of neural tube formation is disrupted, which is an early developmental event. Therefore, whether SIRT1 is involved in environmental stress-induced NTDs remained to be explored. Our study strongly suggests that SIRT1 deacetylase activity is greatly modified by environmental stresses and is responsible for environmental stress-induced abnormal neural induction within the in vitro neural differentiation system of both hESCs and mESCs. Furthermore, in an in vivo radiation-induced NTD model, our results indicated that *Sirt1* very likely translates environmental signals in developing embryos during early neural development and that SIRT1 activation critically contributes to environmental stress-induced NTDs.

Direct competition between lysine acetylation and ubiquitination has been proposed as a major mechanism regulating protein stability and has primarily been documented in cancer progression. p53, E2F1, SKP2, and MSH2 have been reported to be regulated by lysine acetylation and ubiquitination, which play important roles in DNA repair

Figure 6. Environmental Stresses Equally Target the SIRT1/OCT6 Axis and Hinder Neural Induction of hESCs

(A–C) RSV treatment (30 μM) hinders the neural differentiation of hESCs, as shown by the reduced expression of *N-cadherin*, *Sox1*, *Nestin*, and *Sox2*, which were verified by immunostaining (A and B) and qPCR (C) analysis at day 10 of differentiation.

(D) SIRT1 deacetylase activity is elevated by RSV treatment at day 5.

(E) RSV treatment induces OCT6 downregulation at day 5 and day 6.

(F) *Sirt1* knockout elevates OCT6 protein levels at day 3.

(G) *Sirt1* knockout potentiates the neural differentiation of hESCs, as verified by the increased mRNA levels of neural-lineage genes at day 10.

(H) *Sirt1* knockout rescues the downregulation of OCT6 protein levels induced by RSV treatment at day 5.

(I) *Sirt1* knockout rescues the neural induction defects induced by RSV treatment, as verified by the mRNA levels of neural-lineage genes at day 10.

(J) Overexpression of *Sirt1* hinders the neural differentiation of hESCs, as shown by the reduced levels of neural-lineage genes at day 10.

(K) H_2O_2 (0.1 mM), HU (0.4 μM), and glucose starvation hinder the neural differentiation of hESCs, as shown by the reduced levels of neural-lineage genes at day 10.

Data are shown as means ± SEM of three independent experiments. Unpaired two-tailed Student's t test. *$p < 0.05$, **$p < 0.01$, ***$p < 0.001$ versus the control; $^{\#}p < 0.05$, $^{\#\#}p < 0.01$, $^{\#\#\#}p < 0.001$ versus the RSV-treated wild-type hESC group. Scale bars, 100 μm.

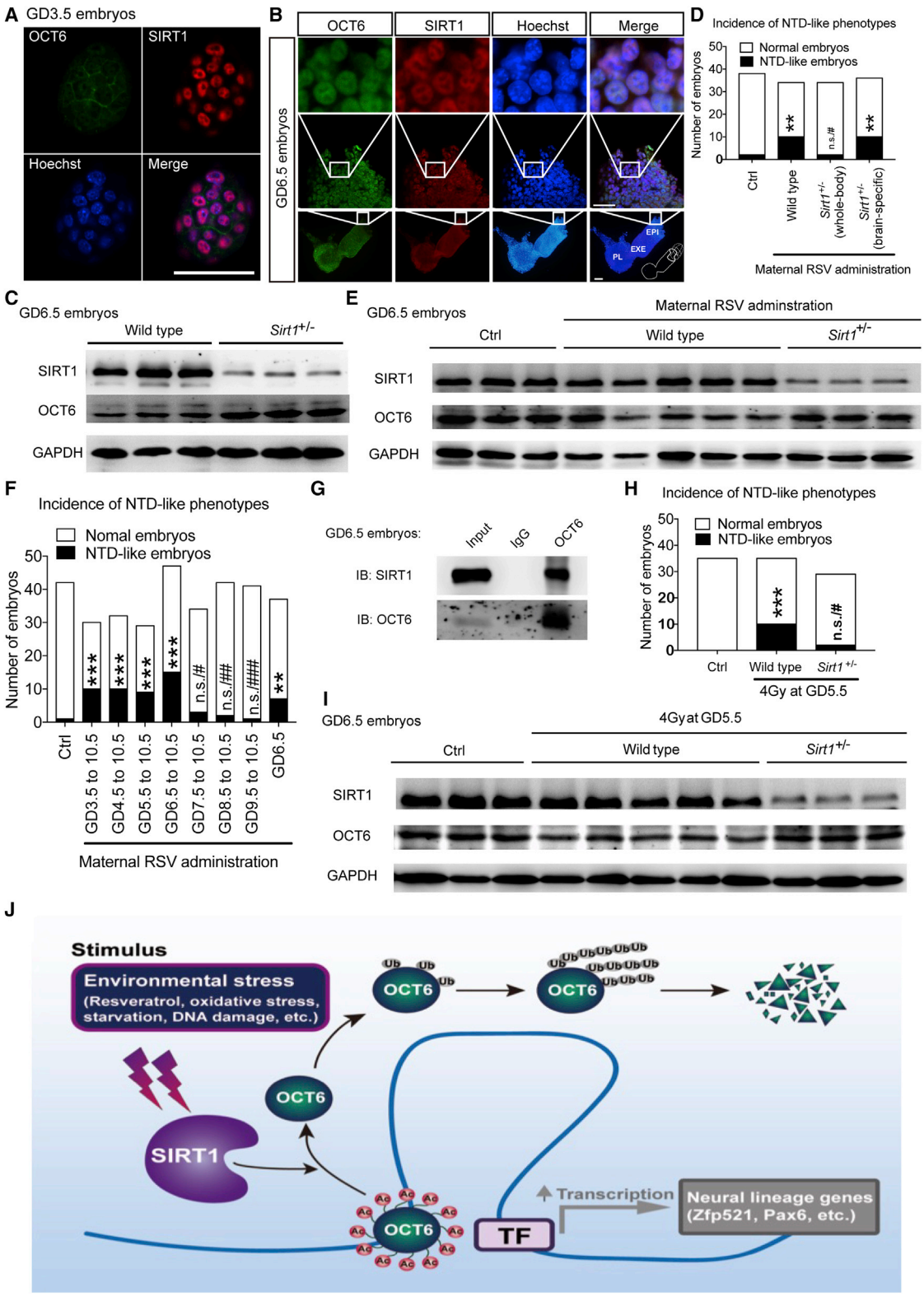

(legend on next page)

and tumorigenesis (Ito et al., 2002; Kontaki and Talianidis, 2010; Wang et al., 2012; Zhang et al., 2014). Recently, the functional relationship between acetylation and ubiquitination was assessed in a study of TAU-mediated neurodegeneration disorders (Min et al., 2015). However, little is known about the role of this post-translational interrelationship in early developmental events, because these events are mostly thought to be transcriptionally regulated. In the present study we discovered the inverse expression of SIRT1 and OCT6, and the active competition between OCT6 acetylation and ubiquitination during mouse gastrulation and the in vitro neural differentiation of both hESCs and mESCs. Notably, we identified a direct physical interaction between SIRT1 and OCT6 both in vivo and in vitro. Although the details regarding the specific OCT6 lysine residues that become acetylated or ubiquitinated remain to be further elucidated, the present study clearly demonstrates that active competition between OCT6 acetylation and ubiquitination is indispensable for normal neural induction.

Mammalian embryonic development is a highly coordinated set of processes involving dramatic but regular changes in the architecture of both the transcriptome and proteome. Previous reports have demonstrated that although the majority of human stage-specific gene expression modules are notably preserved in mouse embryos, the developmental specificity and timing dramatically differ between human and mouse (Xue et al., 2013). Species differences in embryonic development, especially neural induction (Zhang et al., 2010), make animal models suboptimal for studying the etiology and pathology of developmental disorders, including NTDs. In the present study, we clearly identified the direct activation of SIRT1 deacetylase activity upon environmental stress treatment and the resulting degradation of OCT6 protein via deacetylation/ubiquitination cascade during mouse neural differentiation and gastrulation. Importantly, we recapitulated the functional interplay between SIRT1 and OCT6 during human neural induction and found that it coincides exactly with the results from mice. Collectively, our data demonstrated that the developmental role of the SIRT1/OCT6 axis is evolutionarily conserved in both humans and mice; thus, a mouse model targeting the SIRT1/OCT6 axis will facilitate the study of abnormal neural induction in NTDs triggered by environmental stresses. Finally, the regulation of the SIRT1/OCT6 axis may serve as a target for preventing these devastating neurodevelopmental disorders.

EXPERIMENTAL PROCEDURES

Animal Studies

All procedures involving animals were approved by the Laboratory Animal Care Committee of Tongji University under the Guide for the Care and Use of Laboratory Animals (NIH Guide). All mice were maintained in a pathogen-free environment throughout the experiments, and all efforts were made to minimizing the number of animals used and their suffering.

mESC Culture and Neural Differentiation

mESC lines 46C (kindly provided by Austin Smith's laboratory) and R1 (American Type Culture Collection) were maintained on irradiated mouse embryonic fibroblasts with leukemia inhibitory factor (1,000 U/mL, Millipore). For neural differentiation, mESCs were seeded at a density of $(5 \pm 1) \times 10^4$ cells/mL in GK8 medium, as described previously (Watanabe et al., 2005). All the cells were free of mycoplasma contamination.

Induced EpiSC Generation and Neural Differentiation

For generation of induced EpiSCs, mESCs were plated at a density of $(5 \pm 1) \times 10^4$ cells/mL in laminin-coated plates as described previously (Hayashi et al., 2011). For neural differentiation, induced EpiSC clones were dissociated and resuspended in GK8 medium.

Figure 7. The Functional Role of the SIRT1/OCT6 Axis in Environmental Stress-Induced Neural Induction Defect during Early Embryogenesis

(A and B) Immunostaining of SIRT1 and OCT6 in GD3.5 (A) and GD6.5 (B) embryos. EPI, epiblast; EXE, extraembryonic ectoderm; PL, placenta.

(C) OCT6 protein levels in GD6.5 wild-type and *Sirt1*$^{+/-}$ embryos.

(D) The incidence of NTD-like phenotypes in GD10.5 *Sirt1*$^{+/-}$ embryos or brain-specific (*Nestin-Cre*) *Sirt1*$^{+/-}$ embryos after maternal RSV administration.

(E) OCT6 protein levels in wild-type or *Sirt1*$^{+/-}$ embryos with or without maternal RSV administration.

(F) The incidence of NTD-like phenotypes in GD10.5 embryos after applying RSV administration from different gestational days.

(G) The physical interaction between SIRT1 and OCT6 in GD6.5 embryos. IgG, immunoglobulin G; IB, immunoblot.

(H) The incidence of NTD-like phenotypes in GD10.5 wild-type or *Sirt1*$^{+/-}$ embryos with or without 4 Gy radiation at GD5.5.

(I) OCT6 protein levels in GD6.5 wild-type or *Sirt1*$^{+/-}$ embryos with or without radiation.

(J) Schematic representation of the role of SIRT1 in sensing environmental stresses and antagonizing neural induction by deacetylating OCT6 and inducing its ubiquitination/degradation.

Data were analyzed by Chi-square test. n.s. (not significant), $p > 0.05$; $^{**}p < 0.01$, $^{***}p < 0.001$ versus the untreated control; $^{\#}p < 0.05$, $^{\#\#}p < 0.01$, $^{\#\#\#}p < 0.001$ versus the RSV-treated wild-type embryos (D), RSV administration from GD6.5 to GD10.5 (F), and radiation-treated wild-type embryos (H). Scale bars, 50 μm.

hESC Culture and Neural Differentiation

The culture and neural differentiation of hESCs (H9, WA09, passages 25–45, WiCell Agreement No. 14-W0377) were performed as described previously (Zhang and Zhang, 2010).

mRNA Extraction and qPCR

Total RNAs were isolated from the desired cells using the TRIzol (Invitrogen), reverse transcribed into cDNA using SuperScript III First-Strand Synthesis System (Invitrogen), and subjected to qRT-PCR (Bio-Rad, CFX Connect Real-Time System) with the SYBR Premix Ex Taq (TakaRa). The primers used for qPCR are listed in Table S1.

Statistical Analysis

All statistical data are presented as the mean ± SEM of at least three independent experiments. Statistical significance was determined using unpaired two-tailed Student's t tests, except when specially noted otherwise.

SUPPLEMENTAL INFORMATION

Supplemental Information includes Supplemental Experimental Procedures, seven figures, and one table and can be found with this article online at http://dx.doi.org/10.1016/j.stemcr.2017.03.017.

AUTHOR CONTRIBUTIONS

All authors discussed the experiments and contributed to the text of the manuscript. G.L. conducted most of the experiments and wrote a draft of the manuscript. Z.J. and R.W. contributed to plasmid construction and data collection. Z.J. and Y.H. contributed to the gene-editing studies. W.J., J.X., G.W., S.Z., Xin Zhang, D.F., and L.L. discussed the manuscript extensively and contributed to project conception and design. G.L., Xiaoqing Zhang, and J.K. conceived the project, analyzed the data, and wrote the manuscript.

ACKNOWLEDGMENTS

The authors wish to thank Prof. Jun Xu for the transgenic mice. This work was supported by grants obtained from the Ministry of Science and Technology (grant numbers 2016YFA0101300, 2013CB967600, 2013CB967401, 2012CB966603), the National Natural Science Foundation of China (grant numbers 81530042, 31210103905, 31471250, 31371510, 31571519, 31571529, 31671533, 31571390, 31401257, 31401126, 31301213), the Ministry of Education Grant IRT_15R51, the Science and Technology Commission of Shanghai Municipality (grant numbers 15JC1403200, 15JC1400202), and the Fundamental Research Funds for the Central Universities (20002310002, 2000219136, 1507219042, 1500219106).

Received: July 29, 2016
Revised: March 14, 2017
Accepted: March 15, 2017
Published: April 20, 2017

REFERENCES

Acampora, D., Di Giovannantonio, L.G., and Simeone, A. (2013). Otx2 is an intrinsic determinant of the embryonic stem cell state and is required for transition to a stable epiblast stem cell condition. Development *140*, 43–55.

Brunet, A., Sweeney, L.B., Sturgill, J.F., Chua, K.F., Greer, P.L., Lin, Y., Tran, H., Ross, S.E., Mostoslavsky, R., Cohen, H.Y., et al. (2004). Stress-dependent regulation of FOXO transcription factors by the SIRT1 deacetylase. Science *303*, 2011–2015.

Chang, C., Su, H., Zhang, D., Wang, Y., Shen, Q., Liu, B., Huang, R., Zhou, T., Peng, C., Wong, C.C., et al. (2015). AMPK-dependent phosphorylation of GAPDH triggers sirt1 activation and is necessary for autophagy upon glucose starvation. Mol. Cell *60*, 930–940.

Chi, L., Fan, B., Zhang, K., Du, Y., Liu, Z., Fang, Y., Chen, Z., Ren, X., Xu, X., Jiang, C., et al. (2016). Targeted differentiation of regional ventral neuroprogenitors and related neuronal subtypes from human pluripotent stem cells. Stem Cell Rep. *7*, 941–954.

Cho, A., Tang, Y., Davila, J., Deng, S., Chen, L., Miller, E., Wernig, M., and Graef, I.A. (2014). Calcineurin signaling regulates neural induction through antagonizing the BMP pathway. Neuron *82*, 109–124.

Cong, L., Ran, F.A., Cox, D., Lin, S., Barretto, R., Habib, N., Hsu, P.D., Wu, X., Jiang, W., Marraffini, L.A., et al. (2013). Multiplex genome engineering using CRISPR/Cas systems. Science *339*, 819–823.

Copp, A.J., Greene, N.D., and Murdoch, J.N. (2003). The genetic basis of mammalian neurulation. Nat. Rev. Genet. *4*, 784–793.

Fairbridge, N.A., Dawe, C.E., Niri, F.H., Kooistra, M.K., King-Jones, K., and McDermid, H.E. (2010). Cecr2 mutations causing exencephaly trigger misregulation of mesenchymal/ectodermal transcription factors. Birth Defects Res. A Clin. Mol. Teratol. *88*, 619–625.

Han, M.K., Song, E.K., Guo, Y., Ou, X., Mantel, C., and Broxmeyer, H.E. (2008). SIRT1 regulates apoptosis and Nanog expression in mouse embryonic stem cells by controlling p53 subcellular localization. Cell Stem Cell *2*, 241–251.

Harris, M.J., and Juriloff, D.M. (2010). An update to the list of mouse mutants with neural tube closure defects and advances toward a complete genetic perspective of neural tube closure. Birth Defects Res. A Clin. Mol. Teratol. *88*, 653–669.

Hayashi, K., Ohta, H., Kurimoto, K., Aramaki, S., and Saitou, M. (2011). Reconstitution of the mouse germ cell specification pathway in culture by pluripotent stem cells. Cell *146*, 519–532.

Herrera-Araujo, D. (2016). Folic acid advisories: a public health challenge? Health Econ. *25*, 1104–1122.

Hsieh, C.L., Chen, K.C., Ding, C.Y., Tsai, W.J., Wu, J.F., and Peng, C.C. (2013). Valproic acid substantially downregulated genes folr1, IGF2R, RGS2, COL6A3, EDNRB, KLF6, and pax-3, N-acetylcysteine alleviated most of the induced gene alterations in chicken embryo model. Rom. J. Morphol. Embryol. *54*, 993–1004.

Ito, A., Kawaguchi, Y., Lai, C.H., Kovacs, J.J., Higashimoto, Y., Appella, E., and Yao, T.P. (2002). MDM2-HDAC1-mediated deacetylation of p53 is required for its degradation. EMBO J. *21*, 6236–6245.

Kamiya, D., Banno, S., Sasai, N., Ohgushi, M., Inomata, H., Watanabe, K., Kawada, M., Yakura, R., Kiyonari, H., Nakao, K., et al. (2011). Intrinsic transition of embryonic stem-cell differentiation into neural progenitors. Nature *470*, 503–509.

Kang, H., Jung, J.W., Kim, M.K., and Chung, J.H. (2009). CK2 is the regulator of SIRT1 substrate-binding affinity, deacetylase activity and cellular response to DNA-damage. PLoS One *4*, e6611.

Kontaki, H., and Talianidis, I. (2010). Lysine methylation regulates E2F1-induced cell death. Mol. Cell *39*, 152–160.

Koyama, Y., Banzai, T., Sonezaki, S., and Kusano, K. (2006). Stable expression of a heterogeneous gene introduced via gene targeting into the HPRT locus of human fibrosarcoma cells. Biotechnol. Bioeng. *95*, 1052–1060.

Lee, I.H., Cao, L., Mostoslavsky, R., Lombard, D.B., Liu, J., Bruns, N.E., Tsokos, M., Alt, F.W., and Finkel, T. (2008). A role for the NAD-dependent deacetylase Sirt1 in the regulation of autophagy. Proc. Natl. Acad. Sci. USA *105*, 3374–3379.

Liu, L., Liu, X., Ren, X., Tian, Y., Chen, Z., Xu, X., Du, Y., Jiang, C., Fang, Y., Liu, Z., et al. (2016a). Smad2 and Smad3 have differential sensitivity in relaying TGFbeta signaling and inversely regulate early lineage specification. Sci. Rep. *6*, 21602.

Liu, Z., Hui, Y., Shi, L., Chen, Z., Xu, X., Chi, L., Fan, B., Fang, Y., Liu, Y., Ma, L., et al. (2016b). Efficient CRISPR/Cas9-mediated versatile, predictable, and donor-free gene knockout in human pluripotent stem cells. Stem Cell Rep. *7*, 496–507.

Luo, J., Nikolaev, A.Y., Imai, S., Chen, D., Su, F., Shiloh, A., Guarente, L., and Gu, W. (2001). Negative control of p53 by Sir2alpha promotes cell survival under stress. Cell *107*, 137–148.

Min, S.W., Chen, X., Tracy, T.E., Li, Y., Zhou, Y., Wang, C., Shirakawa, K., Minami, S.S., Defensor, E., Mok, S.A., et al. (2015). Critical role of acetylation in tau-mediated neurodegeneration and cognitive deficits. Nat. Med. *21*, 1154–1162.

Nagai, T., Aruga, J., Minowa, O., Sugimoto, T., Ohno, Y., Noda, T., and Mikoshiba, K. (2000). Zic2 regulates the kinetics of neurulation. Proc. Natl. Acad. Sci. USA *97*, 1618–1623.

Pallas, M., Casadesus, G., Smith, M.A., Coto-Montes, A., Pelegri, C., Vilaplana, J., and Camins, A. (2009). Resveratrol and neurodegenerative diseases: activation of SIRT1 as the potential pathway towards neuroprotection. Curr. Neurovasc. Res. *6*, 70–81.

Prozorovski, T., Schulze-Topphoff, U., Glumm, R., Baumgart, J., Schroter, F., Ninnemann, O., Siegert, E., Bendix, I., Brustle, O., Nitsch, R., et al. (2008). Sirt1 contributes critically to the redox-dependent fate of neural progenitors. Nat. Cell Biol. *10*, 385–394.

Salih, M.A., Murshid, W.R., and Seidahmed, M.Z. (2014). Epidemiology, prenatal management, and prevention of neural tube defects. Saudi Med. J. *35* (*Suppl 1*), S15–S28.

Stavridis, M.P., Lunn, J.S., Collins, B.J., and Storey, K.G. (2007). A discrete period of FGF-induced Erk1/2 signalling is required for vertebrate neural specification. Development *134*, 2889–2894.

Stein, L.R., and Imai, S. (2014). Specific ablation of Nampt in adult neural stem cells recapitulates their functional defects during aging. EMBO J. *33*, 1321–1340.

Tam, P.P., and Zhou, S.X. (1996). The allocation of epiblast cells to ectodermal and germ-line lineages is influenced by the position of the cells in the gastrulating mouse embryo. Dev. Biol. *178*, 124–132.

Wang, Z., Inuzuka, H., Zhong, J., Liu, P., Sarkar, F.H., Sun, Y., and Wei, W. (2012). Identification of acetylation-dependent regulatory mechanisms that govern the oncogenic functions of Skp2. Oncotarget *3*, 1294–1300.

Watanabe, K., Kamiya, D., Nishiyama, A., Katayama, T., Nozaki, S., Kawasaki, H., Watanabe, Y., Mizuseki, K., and Sasai, Y. (2005). Directed differentiation of telencephalic precursors from embryonic stem cells. Nat. Neurosci. *8*, 288–296.

Wood, J.G., Rogina, B., Lavu, S., Howitz, K., Helfand, S.L., Tatar, M., and Sinclair, D. (2004). Sirtuin activators mimic caloric restriction and delay ageing in metazoans. Nature *430*, 686–689.

Xue, Z., Huang, K., Cai, C., Cai, L., Jiang, C.Y., Feng, Y., Liu, Z., Zeng, Q., Cheng, L., Sun, Y.E., et al. (2013). Genetic programs in human and mouse early embryos revealed by single-cell RNA sequencing. Nature *500*, 593–597.

Ying, Q.L., Nichols, J., Chambers, I., and Smith, A. (2003a). BMP induction of Id proteins suppresses differentiation and sustains embryonic stem cell self-renewal in collaboration with STAT3. Cell *115*, 281–292.

Ying, Q.L., Stavridis, M., Griffiths, D., Li, M., and Smith, A. (2003b). Conversion of embryonic stem cells into neuroectodermal precursors in adherent monoculture. Nat. Biotechnol. *21*, 183–186.

Yoo, Y.D., Huang, C.T., Zhang, X., Lavaute, T.M., and Zhang, S.C. (2011). Fibroblast growth factor regulates human neuroectoderm specification through ERK1/2-PARP-1 pathway. Stem Cells *29*, 1975–1982.

Zhang, X.Q., and Zhang, S.C. (2010). Differentiation of neural precursors and dopaminergic neurons from human embryonic stem cells. Methods Mol. Biol. *584*, 355–366.

Zhang, X., Huang, C.T., Chen, J., Pankratz, M.T., Xi, J., Li, J., Yang, Y., Lavaute, T.M., Li, X.J., Ayala, M., et al. (2010). Pax6 is a human neuroectoderm cell fate determinant. Cell Stem Cell *7*, 90–100.

Zhang, M., Xiang, S., Joo, H.Y., Wang, L., Williams, K.A., Liu, W., Hu, C., Tong, D., Haakenson, J., Wang, C., et al. (2014). HDAC6 deacetylates and ubiquitinates MSH2 to maintain proper levels of MutSalpha. Mol. Cell *55*, 31–46.

Zhou, C., Yang, X., Sun, Y., Yu, H., Zhang, Y., and Jin, Y. (2016). Comprehensive profiling reveals mechanisms of SOX2-mediated cell fate specification in human ESCs and NPCs. Cell Res. *26*, 171–189.

Zhu, Q., Song, L., Peng, G., Sun, N., Chen, J., Zhang, T., Sheng, N., Tang, W., Qian, C., Qiao, Y., et al. (2014). The transcription factor Pou3f1 promotes neural fate commitment via activation of neural lineage genes and inhibition of external signaling pathways. Elife *3*, e02224.

Zwart, R., Broos, L., Grosveld, G., and Meijer, D. (1996). The restricted expression pattern of the POU factor Oct-6 during early development of the mouse nervous system. Mech. Dev. *54*, 185–194.

Stem Cell Reports, Volume *8*

Supplemental Information

Dysregulation of the SIRT1/OCT6 Axis Contributes to Environmental Stress-Induced Neural Induction Defects

Guoping Li, Zeyidan Jiapaer, Rong Weng, Yi Hui, Wenwen Jia, Jiajie Xi, Guiying Wang, Songcheng Zhu, Xin Zhang, Dandan Feng, Ling Liu, Xiaoqing Zhang, and Jiuhong Kang

SUPPLEMENTAL FIGURES

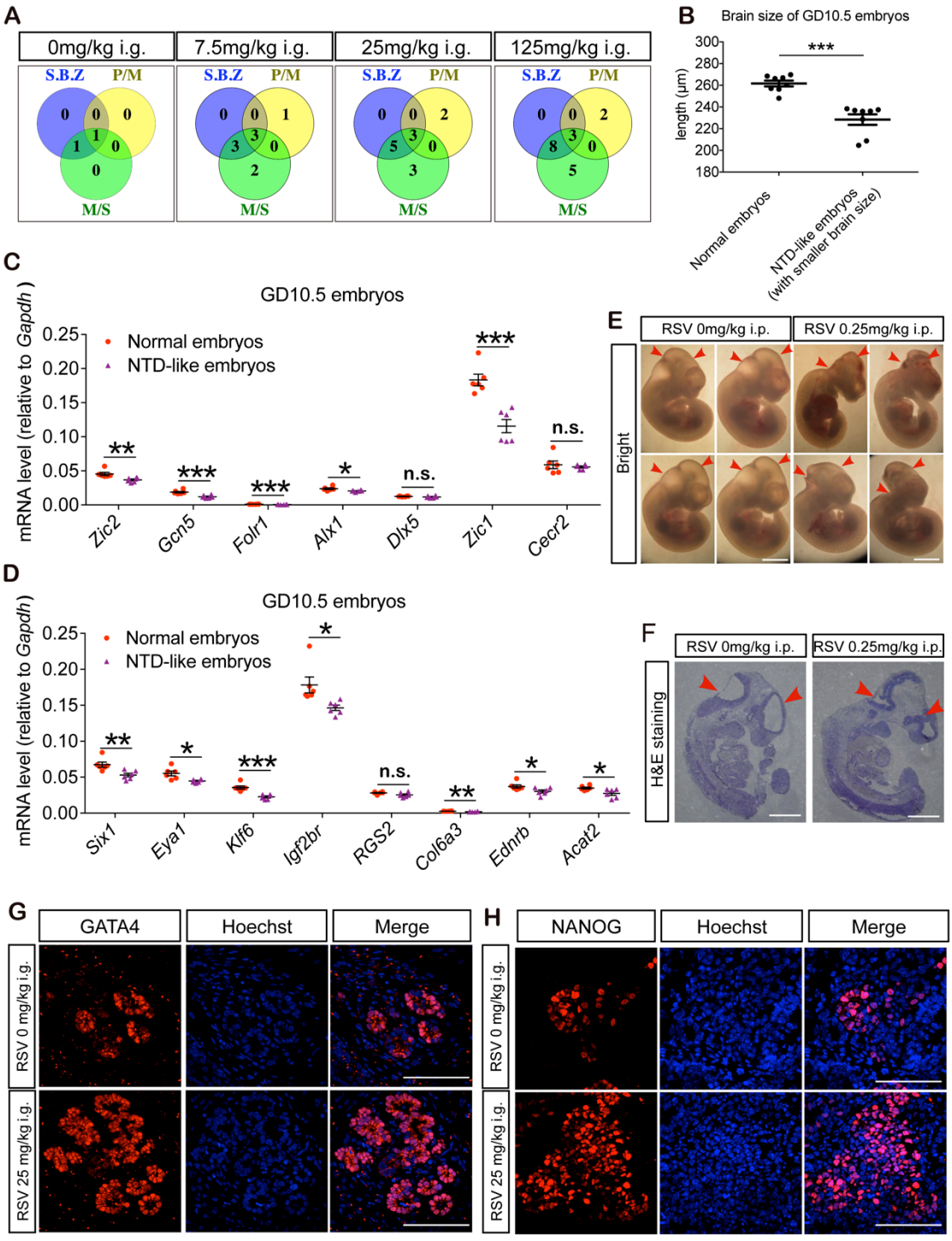

Figure S1. RSV Induces NTD-like Phenotypes *In Vivo*, Related to Figure 1.

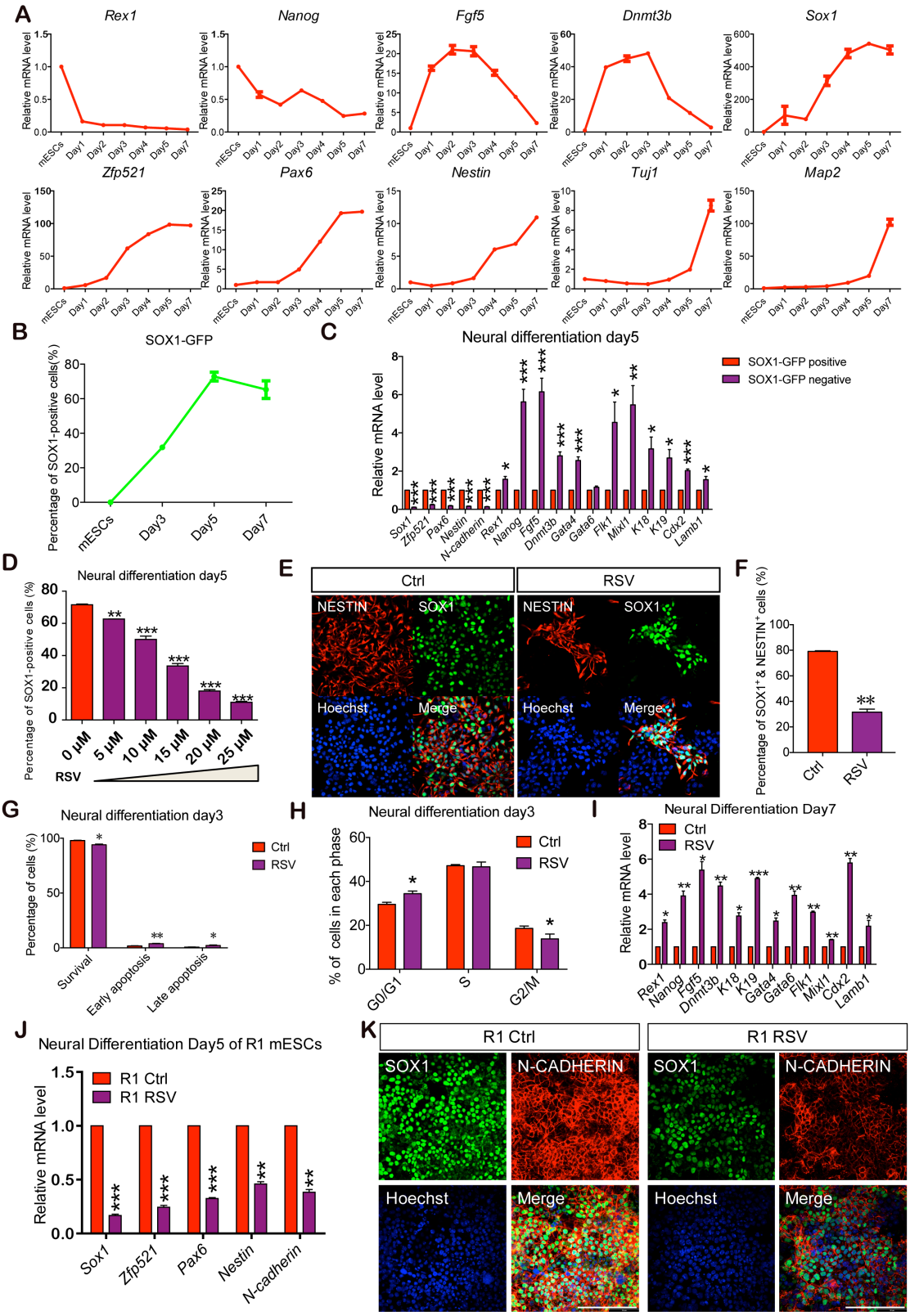

Figure S2. RSV Hinders the Neural Differentiation of mESCs *In Vitro*, Related to Figure 2.

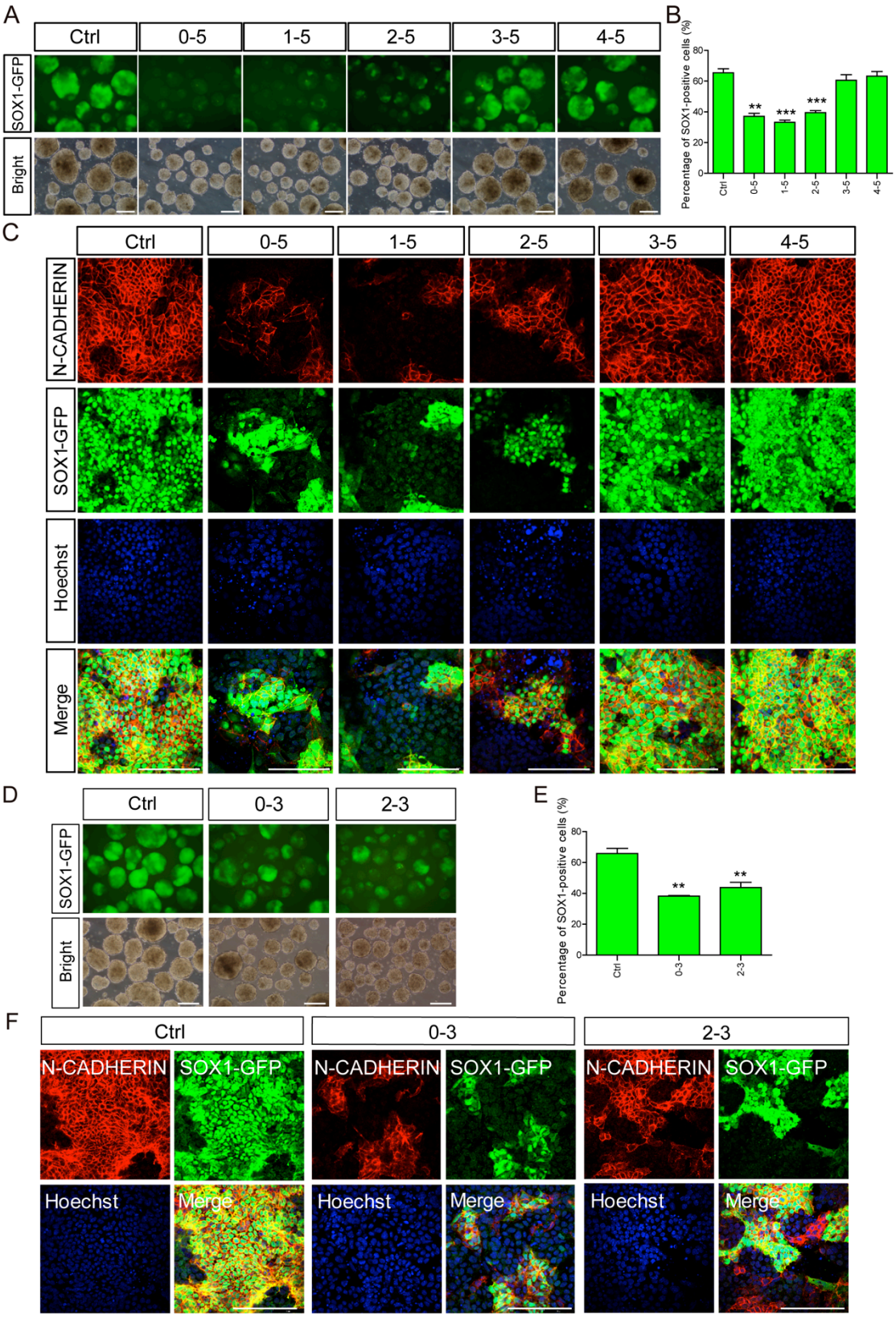

Figure S3. RSV Specifically Hinders the Neural Induction Process During Neural Differentiation, Related to Figure 2.

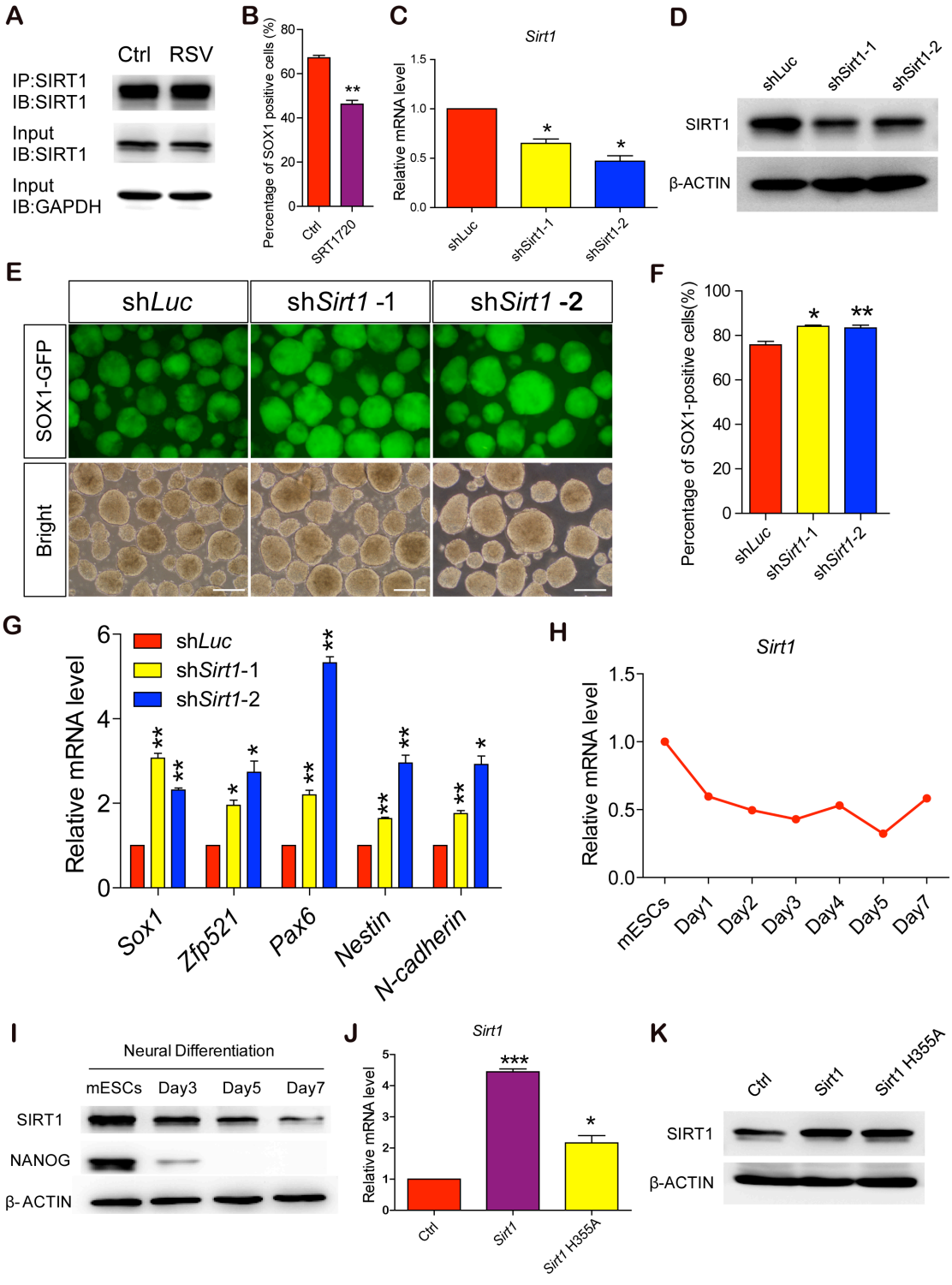

Figure S4. Targeting *Sirt1* in mESCs and the Negative Correlation Between *Sirt1* Expression and Neural Induction Efficiency, Related to Figure 3.

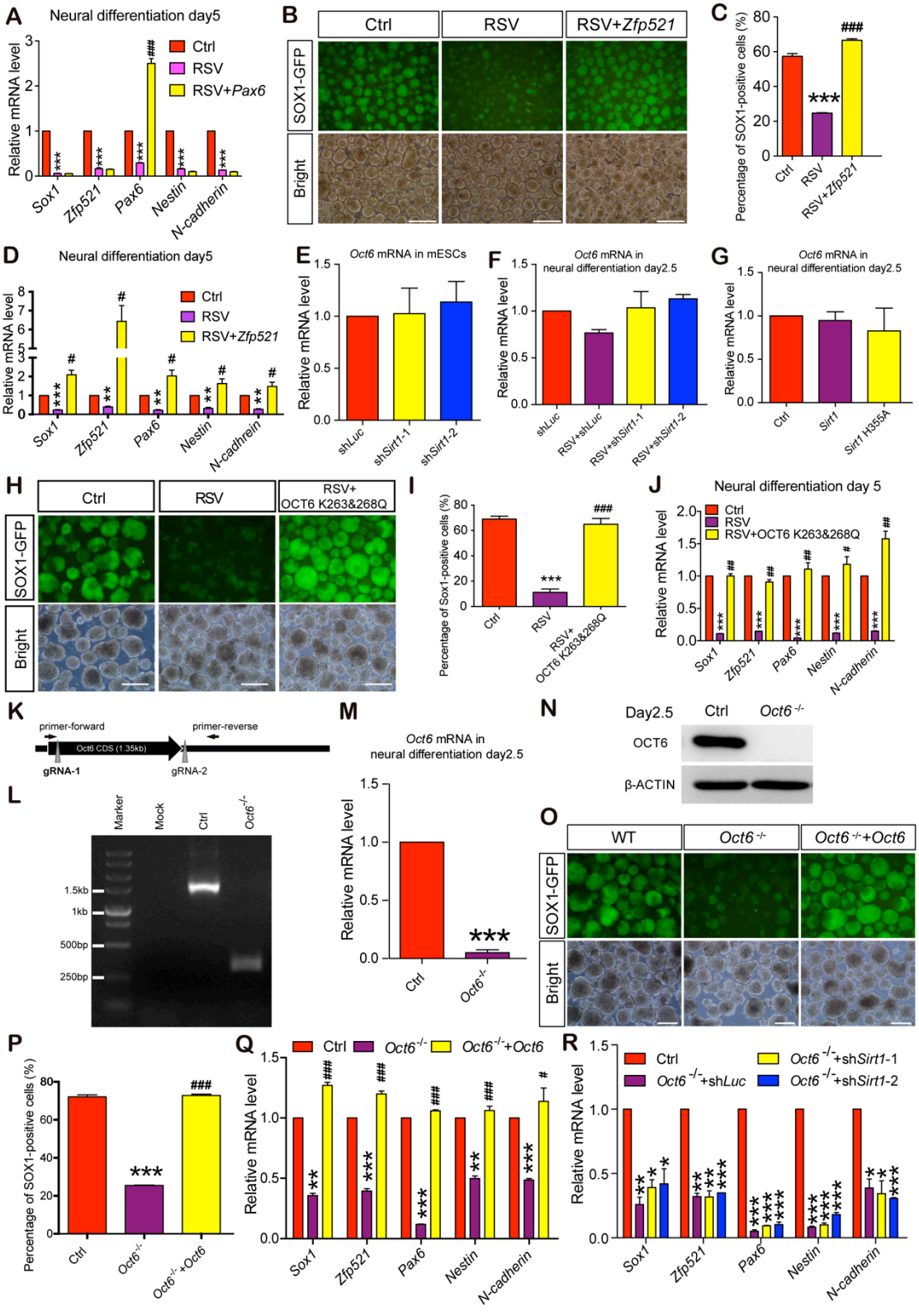

Figure S5. The *Oct6/Zfp521* Pathway is Truly Responsible for the Neural Induction Defects Triggered by RSV Treatment, Related to Figure 4.

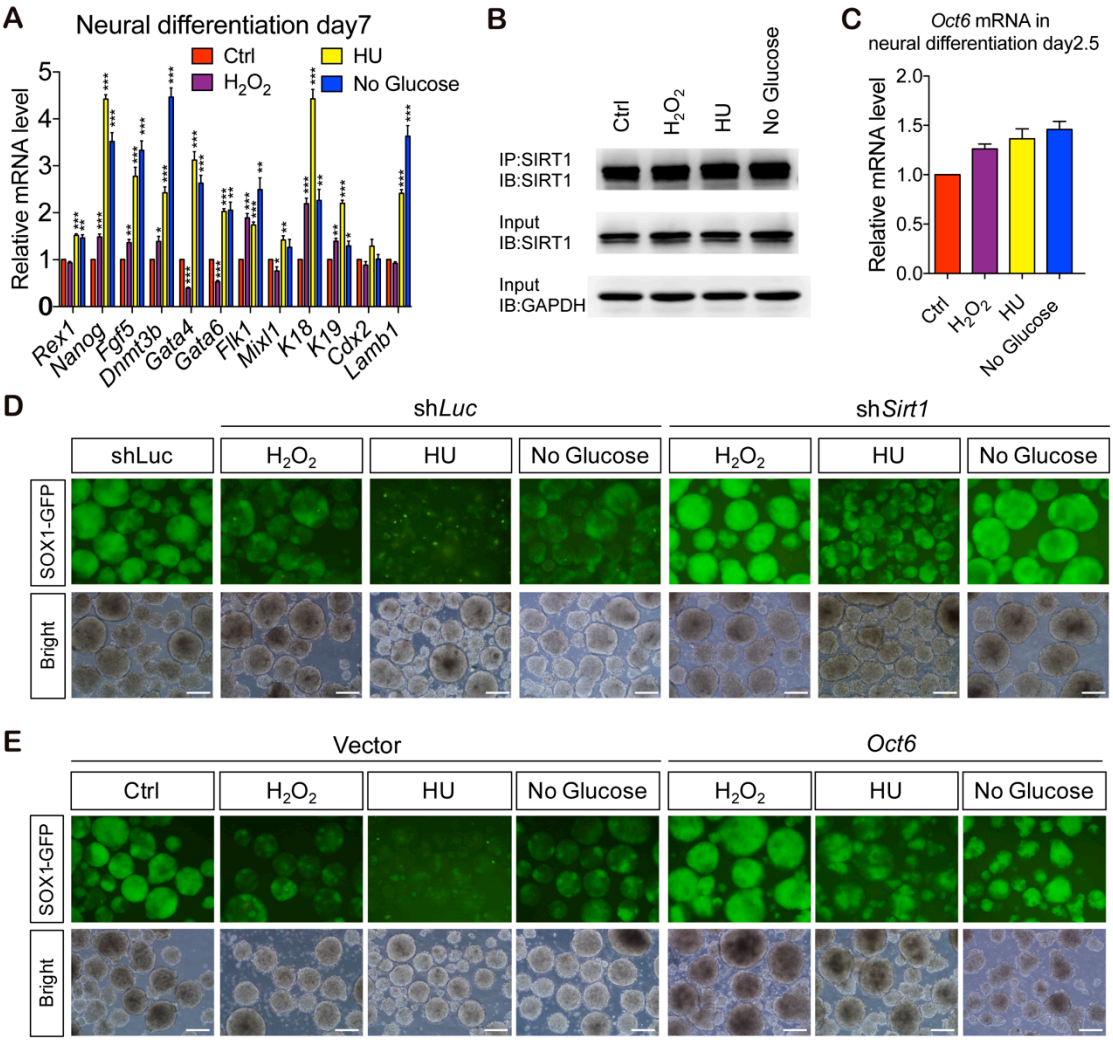

Figure S6. The SIRT1/OCT6 Axis is Required for the Induction of Neural Induction Defects by Environmental Stresses, Related to Figure 5.

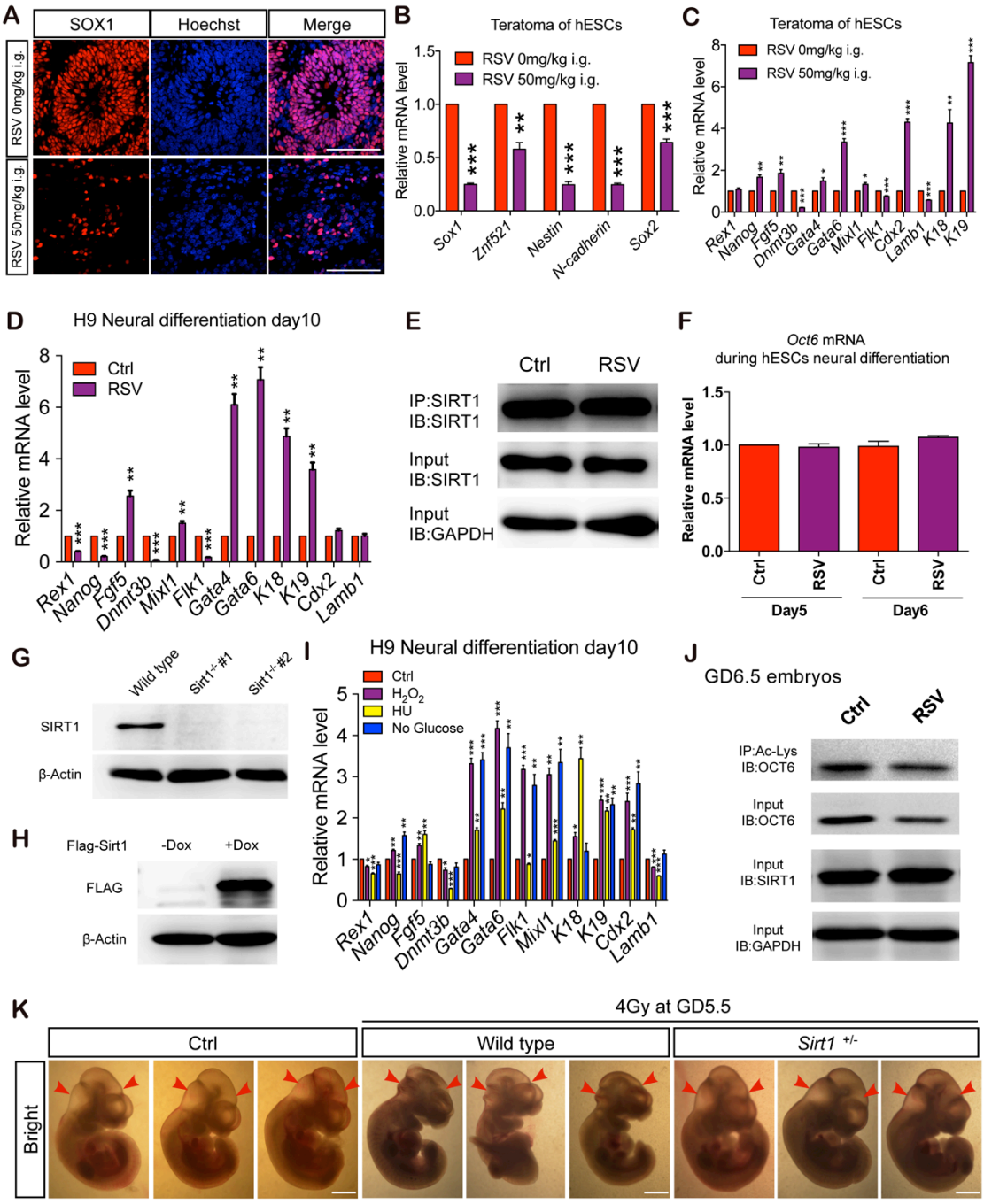

Figure S7. The Functional Role of the SIRT1/OCT6 Axis is Conserved in Humans and is Recapitulated in Radiation-induced NTDs, Related to Figure 6 and 7.

SUPPLEMENTAL FIGURE LEGENDS

Figure S1. RSV Induces NTD-like Phenotypes *In Vivo*, Related to Figure 1.

(A) The number of embryos exhibiting each neurological malformation, including smaller brain size (S.B.Z.), increased indentations between the prosencephalon/metencephalon (P/M) or metencephalon/spinal cord (M/S), after maternal different dosages of RSV administration.
(B) The brain sizes (length from prosencephalon to metencephalon) of normal embryos and RSV-induced NTD-like embryos that exhibit a smaller brain size.
(C and D) The expression level of NTD-risk genes in GD10.5 normal embryos and RSV-induced NTD-like embryos.
(E) Maternal intraperitoneal (i.p.) RSV delivery from GD3.5 to GD10.5 similarly induces NTD-like phenotypes in embryos at GD10.5. Red arrowheads indicate the prosencephalon/metencephalon and metencephalon/spinal cord junctions.
(F) Representative H&E staining of embryos in (E).
(G and H) Immunostaining of GATA4 (G) and NANOG (H) in mouse teratomas with or without RSV administration.
Data are shown as the means ± SEM of at least three independent experiments. Unpaired two-tailed Student's *t*-test. n.s. $p>0.05$, * $p<0.05$, ** $p<0.01$, *** $p<0.001$ versus the control. Scale bar, 100 μm.

Figure S2. RSV Hinders the Neural Differentiation of mESCs *In Vitro*, Related to Figure 2.

(A) Sequential downregulation and activation of pluripotent genes, epiblast genes, neuroepithelial genes and neuronal genes during the neural differentiation of 46C mESCs.
(B) FACS analysis showing the increased expression of the GFP reporter construct during the neural differentiation of 46C mESCs.
(C) Expression level of germ-layer genes in SOX1-GFP-negative or positive cells.
(D) RSV hinders the neural differentiation of 46C mESCs in a dose-dependent manner.
(E) RSV significantly suppresses the formation of neural stem cells, which were labeled by SOX1 and NESTIN.
(F) Formation rate of neural stem cells in (E).
(G and H) RSV treatment slightly affects the apoptosis (G) or cell cycle (H) of differentiated mESCs.
(I) RSV treatment elevates the expression of non-neural-lineage genes.
(J and K) RSV treatment (30 μM) similarly hinders the neural differentiation of R1 mESCs, as shown by Q-PCR (J) and immunostaining (K) analysis in day 5 SFEBs.
Data are shown as the means ± SEM of three independent experiments. Unpaired two-tailed Student's *t*-test. * $p<0.05$, ** $p<0.01$, *** $p<0.001$ versus the control. Scale bar, 100 μm.

Figure S3. RSV Specifically Hinders the Neural Induction Process During Neural Differentiation, Related to Figure 2.

(A-C) RSV was applied to differentiated mESCs at the indicated time points until day 5, and the most significant suppression of neural differentiation was achieved when RSV was added at day 0, 1 and 2, as shown by microscopy (A), FACS (B), and immunostaining (C) analysis in day 5 SFEBs.
(D-F) RSV treatment, from days 0 to 3 or days 2 to 3, is sufficient to inhibit neural differentiation, as shown by microscopy (D), FACS (E), and immunostaining (F) analysis in day 5 SFEBs.
Data are shown as the means ± SEM of three independent experiments. Unpaired two-tailed Student's *t*-test. ** $p<0.01$, *** $p<0.001$ versus the control. Scale bar, 100 μm.

Figure S4. Targeting *Sirt1* in mESCs and the Negative Correlation Between *Sirt1* Expression and Neural Induction Efficiency, Related to Figure 3.

(A) RSV treatment has no obvious effects on SIRT1 protein levels in day 2.5 SFEBs.
(B) FACS analysis showing that the generation of SOX1-GFP-positive neural-lineage cells is inhibited by SRT1720 treatment.
(C and D) *Sirt1* knockdown efficiency, as verified by Q-PCR (C) and western blotting (D).
(E-G) Knocking down *Sirt1* potentiates the neural differentiation of mESCs, as shown by microscopy (E), FACS (F) and Q-PCR (G) analysis in day 5 SFEBs.
(H and I) *Sirt1* mRNA (H) and protein (I) levels are gradually downregulated during neural differentiation.

(J and K) *Sirt1* and *Sirt1* H355A overexpression efficiency, as verified by Q-PCR (J) and western blotting (K).
Data are shown as the means ± SEM of three independent experiments. Unpaired two-tailed Student's *t*-test. * $p<0.05$, ** $p<0.01$, *** $p<0.001$ versus the control. Scale bar, 100 μm.

Figure S5. The *Oct6*/*Zfp521* Pathway is Truly Responsible for the Neural Induction Defects Triggered by RSV Treatment, Related to Figure 4.

(A) Overexpression of *Pax6* during neural differentiation using an inducible system, shows no effects on the results of RSV treatment, as shown by Q-PCR analysis.
(B-D) Overexpression of *Zfp521* completely rescues the neural induction defects triggered by RSV treatment, as shown by microscopy (A), FACS (B), and QPCR (C) analysis in day 5 SFEBs
(E-G) *Oct6* mRNA is marginally regulated by *Sirt1* knockdown (E and F) or overexpression (G).
(H-J) Overexpression of the OCT6 K263&268Q mutant completely rescues the neural induction defects triggered by RSV treatment, as shown by microscopy (H), FACS (I), and QPCR (J) analysis in day 5 SFEBs.
(K) Schematic representation of strategies for *Oct6* knockout in mESCs. Double gRNAs were designed to delete the *Oct6* open reading frame.
(L-N) Verification of *Oct6* knockout efficiency in mESCs via genomic DNA PCR (L), Q-PCR (M) and western blotting (N).
(O-Q) *Oct6*$^{-/-}$ mESCs fail to differentiate into neuroectodermal cells, whereas reintroducing *Oct6* rescues the efficiency of neural induction, as demonstrated by microscopy (O), FACS (P) and Q-PCR (Q) analysis in neural differentiation derivatives from mESCs on day 5.
(R) Q-PCR analysis showing that *Sirt1* knockdown fails to ameliorate the neural differentiation defects of *Oct6*$^{-/-}$ mESCs.
Data are shown as the means ± SEM of three independent experiments. Unpaired two-tailed Student's *t*-test. * $p<0.05$, ** $p<0.01$, *** $p<0.001$ versus the control. # $p<0.05$, ### $p<0.001$ versus the RSV-treated group (A, C, D, I and J) or the *Oct6* knockout group (Q and R). Scale bar, 100 μm.

Figure S6. The SIRT1/OCT6 Axis is Required for the Induction of Neural Induction Defects by Other Environmental Stresses, Related to Figure 5.

(A) H_2O_2, HU and glucose starvation elevate the expression of pluripotent and non-neural-lineage genes.
(B) H_2O_2, HU and glucose starvation show no obvious effects on SIRT1 protein levels during the neural induction stage.
(C) H_2O_2, HU and glucose starvation show no obvious effects on *Oct6* mRNA levels.
(D) Microscopy showing that *Sirt1* knockdown ameliorates the neural induction defects triggered by environmental stressors.
(E) Microscopy showing that ectopic *Oct6* expression rescues the neural induction defects triggered by environmental stress stimulation.
Data are shown as the means ± SEM of three independent experiments. Unpaired two-tailed Student's *t*-test. * $p<0.05$, ** $p<0.01$, *** $p<0.001$ versus the untreated control. Scale bar, 100 μm.

Figure S7. The Functional Role of the SIRT1/OCT6 Axis is Conserved in Humans and is Recapitulated in Radiation-Induced NTDs, Related to Figure 6 and 7.

(A) Immunostaining of SOX1 in the teratomas of hESCs with or without RSV treatment.
(B and C) Expression levels of neural-lineage (B) and non-neural-lineage genes (C) in the teratomas of hESCs with or without RSV treatment.
(D) RSV treatment elevates the expression of other germ layer genes during the neural differentiation of hESCs.
(E) RSV treatment shows no obvious effects on SIRT1 protein levels in neural-differentiation derivatives from hESCs on day 5.
(F) RSV treatment shows a marginal influence on *Oct6* mRNA levels during the neural differentiation of hESCs.
(G) Western blotting verified the efficiency of *Sirt1* knockout in hESCs.
(H) Western blotting verified the efficiency of *Sirt1* overexpression with the inducible system.
(I) H_2O_2, HU and glucose starvation elevate the expression of other germ-layer genes during the neural differentiation of hESCs.
(J) The acetylation of OCT6 in GD6.5 embryos with or without RSV treatment.

(K) Application of 4 Gy radiation at GD5.5 efficiently induces NTDs in wild-type but not Sirt1$^{+/-}$ embryos.
Data are shown as the means ± SEM of three independent experiments. Unpaired two-tailed Student's *t*-test. * $p<0.05$, ** $p<0.01$, *** $p<0.001$ versus the control. Scale bar, 100 μm.

SUPPLEMENTAL TABLE

Table S1. Primers list, related to EXPERIMENTAL PROCEDURES section

Application	Species	Gene	Forward primer	Reverse primer
QPCR	Mouse	*Gapdh*	ATGACATCAAGAAGGTGGTG	CATACCAGGAAATGAGCTTG
QPCR	Mouse	*Sirt1*	AGAACCACCAAAGCGGAAA	TCCCACAGGAGACAGAAACC
QPCR	Mouse & Human	*Sox1*	GTTTTTTGTAGTTGTTACCGC	GCATTTACAAGAAATAATAC
QPCR	Mouse	*Zfp521*	GAGCGAAGAGGAGTTTTTGG	AGTTCCAAGGTGGAGGTCAC
QPCR	Mouse & Human	*Pax6*	TCTTTGCTTGGGAAATCCG	CTGCCCGTTCAACATCCTTAG
QPCR	Mouse	*Nestin*	GAATGTAGAGGCAGAGAAAACT	TCTTCAAATCTTAGTGGCTCC
QPCR	Mouse & Human	*N-cadherin*	TCCTGATATATGCCCAAGACAA	TGACCCAGTCTCTCTTCTGC
QPCR	Mouse	*Oct6*	AGTTCGCCAAGCAGTTCAAG	TGGTCTGCGAGAACACGTTA
QPCR	Mouse	*Rex1*	GGAAGAAATGCTGAAGGTGGAGAC	AGTCCCCATCCCCTTCAATAGC
QPCR	Mouse & Human	*Nanog*	ATTCTTCCACCAGTCCCAAA	ATCTGCTGGAGGCTGAGGTA
QPCR	Mouse	*Fgf5*	AAAGTCAATGGCTCCCACGAA	GGCACTTGCATGGAGTTTTCC
QPCR	Mouse	*Dnmt3b*	CTCGCAAGGTGTGGGCTTTTGTAAC	CTGGGCATCTGTCATCTTTGCACC
QPCR	Mouse	*K18*	ATGCGCCAGTCTGTGGAG	CCTGAGATTTGGGGGCATC
QPCR	Mouse	*K19*	GGGGGTTCAGTACGCATTGG	GAGGACGAGGTCACGAAGC
QPCR	Mouse	*Gata4*	CCTGGAAGACACCCCAATCTC	AGGTAGTGTCCCGTCCCATCT
QPCR	Mouse	*Gata6*	AATGAATGGACTCAGCCGACC	CCGAGGCACCCCGTGTAA
QPCR	Mouse	*Mixl1*	ACTTTCCAGCTCTTTCAAGAGCC	ATTGTGTACTCCCCAACTTTCCC

QPCR	Mouse	*Flk1*	TTTGGCAAATACAACCCTTCAGA	GCAGAAGATACTGTCACCACC
QPCR	Mouse	*Cdx2*	CCTGCGACAAGGGCTTGTTTAG	TCCCGACTTCCCTTCACCATAC
QPCR	Mouse	*Lamb1*	CCCCAATCTCTGTGAACCATG	GCAATTTGCACCGACACTGA
QPCR	Mouse	*Klf4*	GTGCAGCTTGCAGCAGTAAC	AGCGAGTTGGAAAGGATAAAGTC
QPCR	Mouse	*Oct4*	ACATGAAAGCCCTGCAGAAGGAGCT	GAGAACGCCCAGGGTGAGCC
QPCR	Mouse	*Tuj1*	TAGACCCCAGCGGCAACTAT	GTTCCAGGTTCCAAGTCCACC
QPCR	Mouse & Human	*Map2*	GGTCACAGGGCACCTATTCA	TGTTCACCTTTCAGGACTGC
QPCR	Human	*β-Actin*	GACCTGTACGCCAACACAG	CTCAGGAGGAGCAATGATC
QPCR	Human	*Znf521*	TTCCGAGCAAGTGCAGAAAG	AAGGTTCGAGAGCACACGTTG
QPCR	Human	*Oct6*	GCTCGAGAGCCACTTTCTCA	CCAGGCGCGTATACATCGT
QPCR	Human	*Nestin*	GCCCTGACCACTCCAGTTTA	GGAGTCCTGGATTTCCTTCC
QPCR	Human	*Sox2*	GCCCTGCAGTACAACTCCAT	TGGAGTGGGAGGAAGAGGTA
ChIP-PCR	Mouse	*Zfp521*-E1	GGCATCGATGGAGAAAAAG	CATGCAATGGTATGCTAAAG
ChIP-PCR	Mouse	*Zfp521*-E2	TCATCTGAGGAAAGAGGGAGC	TTGATGGTTGCTGGGAATTG
ChIP-PCR	Mouse	*Zfp521*-E3	AGCCGTTTTGTTTCAATCACG	GGGGGAATCTTTTTGTGAAGC
ChIP-PCR	Mouse	*Pax6*	CTAGATGAGCAGTGAGGGC	CAGCTGCTCTGATTAAGATG

SUPPLEMENTAL EXPERIMENTAL PROCEDURES

Animal Studies

All procedures involving animals were approved by the Laboratory Animal Care Committee of Tongji University under the Guide for the Care and Use of Laboratory Animals (NIH Guide). All mice were maintained in a pathogen-free environment throughout the experiments, and all efforts were made to minimizing the number of animals used and their suffering.

RSV (0 mg/kg/day, 7.5 mg/kg/day, 25 mg/kg/day and 125 mg/kg/day) was intragastrically administered to pregnant mice (6~8 weeks old; male and female ICR or C57BL6 mice were obtained from the National Resource Center of Mutant Mice Model Animal Research Center (NARC), Nanjing

University (NJU), and mated randomly) between GD3.5 and GD10.5. For each RSV dosage, two pregnant mice were randomly chosen for each one of the three independent experiments. Embryos at gestational day 10.5 were then harvested and fixed with 4% formaldehyde solution for 4~8 h at 4°C, followed by dehydration with a sucrose gradient before being submitted to frozen sectioning. To verify the effect of RSV on embryonic neural tube development, RSV was also intraperitoneally injected daily from GD3.5 to GD10.5 at a dosage of 0.25 mg/kg/day.

Teratoma formation analysis of mESCs was performed by subcutaneous injection of $(10\pm2)\times10^5$ mESCs into male NOD-SCID mice (4~6 weeks old; obtained from NARC, NJU). After injection, mice were randomly and blindingly divided into two groups (three mice for each group) and were intragastrically administered 25 mg/kg/day of RSV or an equal amount of water daily. Teratomas were harvested when the size exceeded 2.0 cm in diameter and were fixed in 4% paraformaldehyde for 8~12 h before being submitted to paraffin embedding and sectioning. For the teratoma formation analysis of hESCs, hESCs clusters (300~500 clusters/100 μl) were subcutaneously injected into male NOD-SCID mice. The mice were intragastrically administered 50 mg/kg/day of RSV or an equal amount of water daily for 8 weeks.

Gene Knockdown, Knockout or Overexpression in ESCs

For *Sirt1* knockdown, two shRNAs targeting the CDS of *Sirt1* mRNA were designed (sh*Sirt1*-1, AAGCGGCTTGAGGGTAATCAA; sh*Sirt1*-2, AAGCCAGAGATTGTCTTCTTT) and cloned into the pLKO.1-TRC cloning vector, a gift from David Root (Addgene plasmid # 10878) (Moffat et al., 2006). An shRNA targeting *Luciferase* was also designed as a control (sh*Luc*, TGAAACGATATGGGCTGAATA). For lentivirus packaging, foreign DNA (2 μg) was transfected into HEK 293FT cells (1 well of a 6-well-plate) together with the packaging plasmids, *Pax2* (1.5 μg) and *Vsvg* (1 μg), using the Fugene HD transfection reagent (Roche) according to the manufacturer's recommendations. Supernatant containing the lentiviruses was added to mESCs supplied with 8 μg/ml polybrene.

For constitutive overexpression of *Sirt1* or *Sirt1* H355A, a guide RNA (gRNA) targeting a region close to the stop codon of HPRT (*Hprt* gRNA sequence: AAGGGTCCTCCTACGTTGT) and a donor plasmid containing *T2A-Blasticidin-Sirt1*-CAG cassettes flanked by the 5' and 3' homologous arms were co-electroporated into 46C mESCs using the Gene Pulser Xcell System (Bio-Rad) at 320 V, 200 μF in a 0.4-cm cuvettes (Phenix Research Products), and selected with 5 μg/ml blasticidin (InvivoGen) for 5-7 days. The surviving clones were then picked up for genomic DNA PCR analysis. The cDNA of *Sirt1* and *Sirt1* H355A were subcloned from pAd-Track-*Flag-Sirt1* and pAd-Track-*Flag-Sirt1* H355A, gifts of Pere Puigserver (Addgene plasmids # 8438 and #8439) (Rodgers et al., 2005).

For the inducible overexpression system, advanced *rtTA* driven by the CAG promoter was intergraded into the *Rosa26* or *AAVS1* locus via electroporation using engineered zinc-finger nucleases, as described previously (Perez-Pinera et al., 2012). A lentiviral backbone containing tetracycline response element (TRE)-driven *HA-Oct6*, *HA-Otx2*, *HA-Zic2*, *Flag-Sox2, Flag-Pax6, HA-OCT6 K263&268Q, HA-Zfp521 or Flag-Sirt1* was subcloned and used for virus packaging. Medium containing viral particles was then added to the *rtTA* ESCs line for efficient infection.

For *Oct6* knockout, two gRNAs targeting the major open reading frame of *Oct6* were designed (*Oct6* KO gRNA-1, CTTCTGCACTTCGCGGTACG; *Oct6* KO gRNA-2, GCGCGCTAACTGCGCGCCGG) and cloned as previously described (Aparicio-Prat et al., 2015). The

two gRNAs, the CAS9 expression plasmid and a transient blasticidin-resistance gene-expression plasmid were electroporated into *rtTA* mESCs. The cells were selected with 3-10 μg/ml blasticidin for 3 days, and the surviving clones were picked up for genomic DNA PCR analysis. For *Sirt1* knockout in hESCs, two gRNAs targeting the exon1 of *Sirt1* were designed (*Sirt1* KO gRNA-1, CTCCGCGGCCTCTTGCGGAG; *Sirt1* KO gRNA-2, CCGCCGGCACCTCACGCTCT). Cleavage mediated by these dual gRNAs would produce a premature translational termination codon in exon1.

Chromatin Immunoprecipitation (ChIP) Assays

ChIP assays were performed as previously described (Song et al., 2013). Briefly, the day 2.5 mouse neural differentiation derivatives were dissociated into single cells and cross-linked with 1% formaldehyde for 10 min at room temperature, followed by quenching with 0.125 M glycine. Samples were lysed after two washes with PBS and sonicated to generate DNA fragments of approximately 750 bp in length. Then, the chromatin fragments were immunoprecipitated overnight with anti-OCT6 (1:200, Abcam, ab31766) at 4°C. After dissociation from the immunocomplexes, the immunoprecipitated DNAs were quantified by Q-PCR and normalized against the genomic DNA input prepared before immunoprecipitation. The primers used in ChIP-PCR are listed in Table S1.

Immunostaining

For mouse cells, mouse day 4 SFEBs were dissociated into single cells and plated onto 12-mm coverslips coated with 2% (v/v) Matrigel (BD Biosciences) with approximately $(2\pm0.5)\times10^5$ cells for 12~24 hours. For human cells, human neural differentiation derivatives on day 6 were plated into poly-ornithine coated 12-mm coverslips for 3~4 days. Coverslip cultures were then fixed with 4% paraformaldehyde for 10 min at room temperature. After being washed with PBS, the cells were incubated in a penetrating/blocking buffer (10% donkey serum, 0.2% Triton X-100 in PBS) for 1 h at room temperature followed by overnight primary antibody incubation at 4°C. Next, cells were stained with the fluorescently conjugated secondary antibodies (1:2000, Jackson, West Grove, PA) for 1 hour and with Hoechst 33342 (50μg/ml, Sigma, 14533) for 10 min. The following primary antibodies were used: GFP (1:2000, Invitrogen, A6455), N-CADHERIN (1:2000, BD Biosciences, #610920), SOX1 (1:1000, R&D Systems, AF3369), SOX2 (1:1000, R&D Systems, AF2018), PAX6 (1:1000, Covance, PRB-278P), GATA4 (1:500, Santa Cruz, sc-9053), OCT4 (1:1000, Santa Cruz, sc-5279), NANOG (1:1000, Abcam, ab80892) and NESTIN (1:1000, Millipore, MAB5326; 1:1000, Abcam, ab6142).

FACS analysis

To detect the percentage of SOX1-GFP-positive cells, day 3, day 5 or day 7 SFEBs from 46C were dissociated into single cells with trypsin-EDTA, and neutralized with serum. Then the cells were then resuspended in PBS and submitted to FACS analysis, which were performed on a FACSCalibur (BD Biosciences) operating at 488 nm excitation with standard emission filters. A baseline of fluorescence noise was established with undifferentiated mESCs. For the analyses of the cell cycle or apoptosis, SFEBs from 46C were dissociated into single cells with trypsin-EDTA, and neutralized with serum, as specified by the manufacturer (KeyGEN, KGA105 or KGA511).

Immunoprecipitation Assays

Immunoprecipitation assays were performed as described previously (Song et al., 2013). Briefly,

day 2.5 SFEBs were harvested and lysed with lysis buffer (1% Triton X-100 in 50 mM Tris-HCl, pH7.4 containing 150 mM NaCl, 2 mM Na3VO4, 100 mM NaF and protease inhibitors). Cell lysates were incubated overnight with primary antibody or control normal IgG at 4°C. Then, a 5% BSA (w/v, in lysis buffer) coated 1:1 mixture of Ezview Red Protein A Affinity Gel (Sigma, P6486) and Ezview Red Protein G Affinity Gel (Sigma, E3403) was added into the antibody-containing lysates for 1.5 hours. Beads-antibody-protein mixtures were submitted to Western blotting after adequate washing. The following primary antibodies were used for immunoprecipitation: SIRT1 (1:300, Cell Signaling, #8469), OCT6 (1:300, Abcam, ab31766), Ac-Lys (1:300, Upstate, 05-515), mouse normal IgG (1:300, Millipore, 12-371), and rabbit normal IgG (1:300, Millipore, 12-370). To assess the interaction between exogenously expressed proteins, *Flag*-tagged *Sirt1* or *Sirt1* H355A and *HA*-tagged *Oct6* were co-transfected into HEK 293FT cells, and immunoprecipitations were carried out with Ezview Red Anti-FLAG M2 affinity gel (Sigma, F2426) or Ezview Red Anti-HA affinity gel (Sigma, E6779).

Western Blotting

Cells were harvested and lysed with protease inhibitor-containing RIPA buffer. Protein concentrations were standardized using the Pierce BCA Protein Assay Kit (Thermo Scientific). A total of 15 μg of total proteins was separated by SDS-PAGE, transferred to nitrocellulose membranes (NC), and blotted with the following primary antibodies: SIRT1 (1:3000, Millipore, 07-131), OCT6 (1:2000, Abcam, ab31766), Ac-Lys (1:1000, Cell Signaling, #9441), NANOG (1:2000, Abcam, ab80892), Ac-H3K9 (1:2000, Millipore, 06-942), Ac-H4K16 (1:2000, Millipore, 07-329), Histone 3 (1:2000, Millipore, 05-928), Histone 4 (1:1000, Millipore, 05-858), phospho-ERK1/2 (1:2000, Bioworld, AP0484), ERK1/2 (1:2000, Bioworld, BS6426), phospho-GSK3β (Tyr216) (1:2000, Signalway Antibody, #11301), GSK3β (1:2000, Cell Signaling, #9832), GAPDH (1:3000, Sigma, G9545), phospho-SMAD1/5 (1:2000, Cell Signaling, #9511), SMAD1/5/8 (1:1000, Santa Cruz, sc-6031-R), FLAG (1:3000, Sigma, F1804), HA (1:3000, Abcam, ab9110, or 1:2000, Santa Cruz, sc-805 HRP) and β-ACTIN (1:5000, Sigma, A5316).

Fluorometric SIRT1 Activity Assay

To analyze the endogenous SIRT1 deacetylase activity, SIRT1 was immunoprecipitated with anti-SIRT1 (1:300, Millipore, 07-131) from differentiated day 2.5 mouse or day 5 human neural differentiation derivatives with or without environmental stress stimulation, and incubated with NAD^+ (200 μM) and fluorescently labeled acetylated P53 peptide (20 μM), as specified by the manufacturer (Abcam, ab156065). SIRT1 activity was assessed by measuring the fluorescence emission at 440~460 nm following excitation at 350~380 nm.

SUPPLEMENTAL REFERENCES

Aparicio-Prat, E., Arnan, C., Sala, I., Bosch, N., Guigo, R., and Johnson, R. (2015). DECKO: Single-oligo, dual-CRISPR deletion of genomic elements including long non-coding RNAs. BMC Genomics 16, 846.

Moffat, J., Grueneberg, D.A., Yang, X., Kim, S.Y., Kloepfer, A.M., Hinkle, G., Piqani, B., Eisenhaure, T.M., Luo, B., Grenier, J.K., et al. (2006). A lentiviral RNAi library for human and mouse genes applied to an arrayed viral high-content screen. Cell 124, 1283-1298.

Perez-Pinera, P., Ousterout, D.G., Brown, M.T., and Gersbach, C.A. (2012). Gene targeting to the ROSA26 locus directed by engineered zinc finger nucleases. Nucleic acids research 40, 3741-3752.

Rodgers, J.T., Lerin, C., Haas, W., Gygi, S.P., Spiegelman, B.M., and Puigserver, P. (2005). Nutrient control of glucose homeostasis through a complex of PGC-1alpha and SIRT1. Nature 434, 113-118.

Song, C., Zhu, S., Wu, C., and Kang, J. (2013). Histone deacetylase (HDAC) 10 suppresses cervical cancer metastasis through inhibition of matrix metalloproteinase (MMP) 2 and 9 expression. The Journal of biological chemistry 288, 28021-28033.